Interaction of a Shock Wave with a Water Layer

Andrzej Teodorczyk
Institute of Heat Engineering
Warsaw University of Technology
00-665 Warszawa, Nowowiejska 25, POLAND

and

Joseph E. Shepherd
Graduate Aeronautical Laboratories
California Institute of Technology
Pasadena, CA 91125

Explosion Dynamics Laboratory Report FM2012.002

May 2012. Revision of December 13, 2015

Abstract

The interaction of a shock wave propagating in air with a water surface along which the wave is sliding has been studied experimentally in a shock tube with the use of shadow and direct spark photography. The experiments were performed at 0.25 bar initial pressure in the square (89 $\times$ 89 mm) test section for an 8 mm deep and 130 mm long water layer. The shock Mach number was varied from 1.4 to 2.4. It has been shown that after passage of the shock front over the liquid surface, the liquid–gas interface becomes hydrodynamically unstable and random surface instabilities (ripples) of different structure appear on the surface. As the flow progresses over the surface, a single large-amplitude surface wave is formed with the size and velocity dependent on the flow Mach number. The results also provide information on water spray entrainment into the shock–induced air flow. At low shock Mach number ($1.3 < M_s < 1.6$), the spray is mainly driven from the recirculating region formed by the backward–facing step in the bottom wall of the channel. At higher Mach numbers, the spray is formed from the surface wave and from the entire water surface. When an initial perturbation of the water surface was introduced the rate of spray entrainment was increased, in particular at early times in the interaction process.

Contents

List of Figures

1 Introduction

Shock or detonation waves propagating across a layer of liquid can cause lofting of the liquid in the form of a fine aerosol resulting in a mist or cloud of liquid droplets in the atmosphere above the liquid surface. This can occur if there is an accidental explosion within the headspace gases of a tank containing liquid waste, see Fig. 1. In the case of tanks that contain radioactive material, this is a particularly important concern in safety analyses since the lofted material may pose a serious health hazard. One of the motivations for the present study was to improve our understanding of the lofting process in order to develop improved estimates for the amount of material that is lofted.

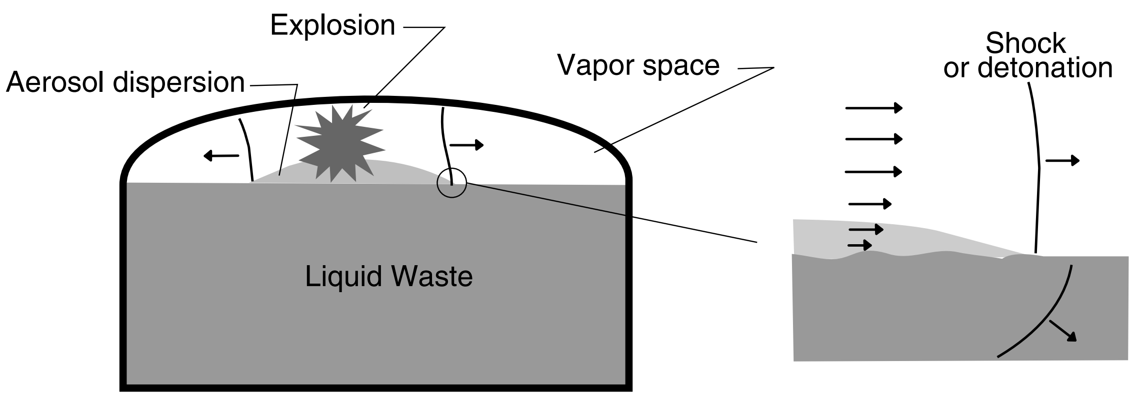

Figure 1: Mechanisms of dispersion associated with explosions inside waste tanks.

From a scientific viewpoint, the propagation of a shock wave across a liquid layer is an example of a class of problems often referred to as "shock wave refraction." The interaction of a shock wave with an interface between two fluids has been extensively studied in the case of gases and the interactions have been classified in terms of the relative density and sound speeds in the two fluids. The interface between a liquid and a gas has many features in common with the gas–gas interface but has been less extensively studied.

There are two cases depending on the relative speed of the shock wave compared to the sound speed in the liquid, see Fig. 2. In the regular refraction case, the shock wave in the air travels faster than the sound speed in the liquid layer. An oblique shock is refracted into the liquid and subsequent reflections from the lower surface of the liquid layer result in a system of oblique waves within the layer. A single reflected wave propagates into the air. The situation is much more complex when the shock wave in the air propagates at a velocity less than the sound speed in the liquid layer. This is the case of irregular refraction. The refracted wave runs out ahead of the shock and a weak oblique precursor is generated in the air in front of the main shock. A weak reflected wave is created behind the main air shock due to the interaction of the precursor with the shock.

1.1 Previous Studies

Previous work on this problem includes the refraction of shocks at a gas-liquid interface (Henderson et al., 1990, Itaka et al., 1989, Yamada et al., 1995) and the dispersion and com-

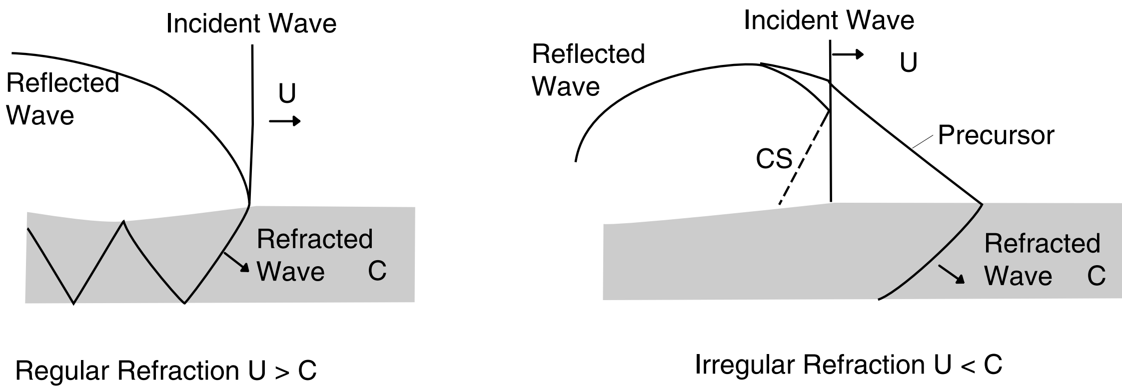

Figure 2: Regular and irregular refraction of a shock wave in air propagating along a water layer.

bustion of fuel layers within shock tubes and combustion engines. Motivated by combustion of thin films of liquid on the walls of tubes carrying flowing air, Borisov et al. (1965a,b, 1968, 1980, 1990) have experimentally studied the stability of various liquids when a shock or detonation wave is sliding along the surface. Borisov et al. determined that in the case of waves moving supersonically relative to the liquid, the liquid surface develops instability with a wavelength corresponding to the system of waves set up by the regular refraction as shown in Fig. 2. For shock waves moving subsonically relative to the liquid, instability of the surface was also observed. In both cases, a fine mist (estimated sizes of less than 2 μm diameter) of droplets was created in liquids such as water, glycerin, kerosene, cetane, and mercury. Borisov et al. (1980) proposed a model of mist formation that is based on the Kelvin-Helmholtz instability of the surface followed by stripping of mist from the waves once they have reached a critical amplitude.

Milton et al. (1992) carried out a study on the lofting thin layers of liquid water, alcohol, cooking oil, and gasoline. In experiments with a geometry similar to the present work, they observed the formation of solitary waves in water and cooking oil for $M_s = 1.315$ shocks.

The present work differs from the previous studies in that we have emphasized the role of the transition from the shock tube wall to the water layer. The production and growth of the solitary wave on the liquid surface has been examined in detail. Previous work has used shadowgraphy with side views. We have used this technique but have also used oblique imaging photography to visualize the 3-D structure of the liquid surface. We have also examined the role of pre-existing disturbances on the surface.

2 Experimental

Experiments were performed in a Caltech 6-in shock tube Smith et al. (1967). This circular shock tube (Fig. 3) has a 1.83 m long driver section and an 11.27 m long driven section separated by a diaphragm. At the end of driven section there is a “cookie cutter” connected to 89 × 89 mm square test section, 0.6 m long, and lastly, a 0.6 m long buffer section. In the experiments, the high-pressure driven section was filled with helium and the low-pressure test section was filled with air at an initial pressure of 0.25 bar. The cavity at the bottom

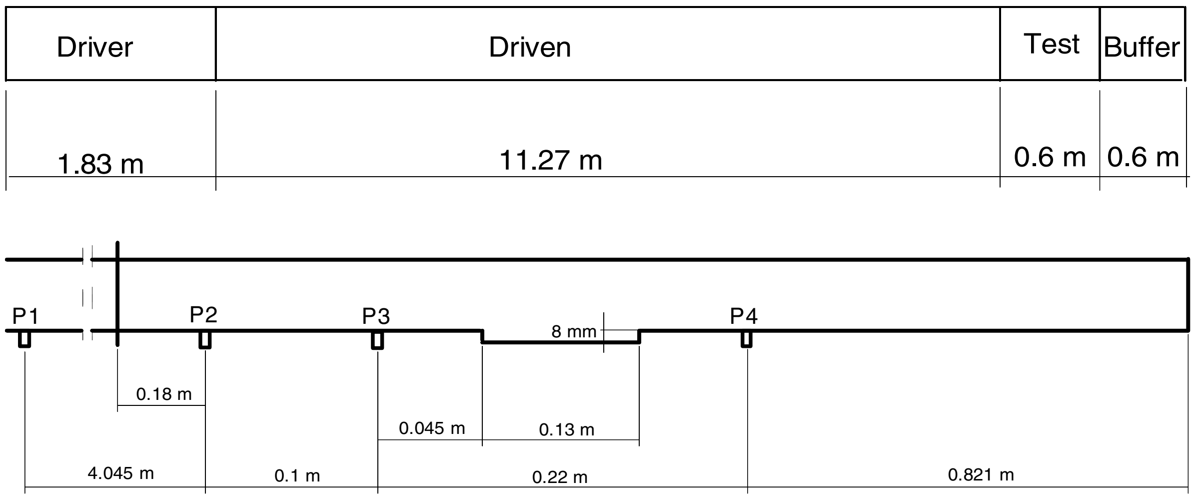

Figure 3: Caltech 6-in shock tube and test section used in this study.

wall of the test section, 130 mm long and 8 mm high, was filled with water. Experiments were carried out with both quiescent and disturbed surfaces. The disturbances were capillary waves created by a vibrating submerged surface.

A shock wave in the air was created by breaking the diaphragm (aluminum sheet) by increasing the helium pressure in the driver section. The rupture process is made repeatable by using a set of curved knife blades just downstream of the diaphragm. By varying the thickness of the aluminum foil diaphragm, shock waves of various shock Mach numbers in the range $1.34 < M_s < 2.4$ were created. Piezoelectric pressure transducers were mounted along the bottom wall to measure the pressure and velocity of the shock wave. The test section was also equipped with glass windows for photographic observations of the shock–water interactions. The events were photographed by a Polaroid camera using a time–delayed spark shadow technique as well as direct photography. Synchronization of the optical system spark with the shock position was achieved via a digital delay generator. The initiation of events originated from a pulse of a pressure transducer marked as P1 in Fig. 3.

3 Results

Figure 4 presents the time sequence of shadow photographs showing the phenomena associated with shock passage along the surface of water and the shock induced air flow. The first picture at 0 ms shows the incident shock of the Mach number $M_s = 2.3$ and the reflected curved wave moving upwards which resulted from shock diffraction at the backward–facing step in the bottom wall of the channel. A number of weak shocks are also visible on the first and second pictures that originate from the incident shock reflections at the small water surface instabilities (ripples) which are induced by the flow behind the shock front. As the flow progresses over the surface, a single large–amplitude, slow–moving surface wave is formed with the size and velocity dependent on the flow Mach number. The photographs also show the dynamics of water spray (fog, mist) entrainment into the shock induced air flow. For the shock Mach number $M_s = 2.3$, the spray is formed from the entire water surface shortly after the passage of the shock front (dark horizontal zone on the third frame) and grows in thickness in time. The last four frames in Fig. 4 clearly show the motion of the single surface wave in the downstream direction.

Figure 5 presents the shadow photographs taken 3 ms after shock passage for different shock Mach numbers in the whole range studied (M_s = 1.34—2.3). These pictures clearly show the dependence of the size and velocity of the water surface wave on flow Mach number. They also show that at low Mach number, the water spray is mainly driven from the recirculation region formed by the backward–facing step of the water cavity, with just a little spray formed at the water surface.

Figure 6 presents the time sequence of shadow photographs for the shock Mach number $M_s = 2.3$ and with the initial perturbations on the water surface introduced by means of a small circular vibrating rod immersed in the water. In this case, a number of shocks are visible in the air; these are created by the diffraction of the incident wave from the wavy water surface. Comparison with Fig. 4 also reveals the increased rate of spray entrainment from a wavy surface as compared to an initially plane surface.

Figure 7 presents the time sequence of direct photographs of the water surface during the air flow induced by a shock wave of Mach number $M_s = 2.3$. The first frame shows the beginning of the formation of the water surface wave and the water spray. The next frames show the increase of the water spray layer thickness and the propagation of the large-amplitude wave downstream. Figure 8 presents the direct photographs taken 2 ms after shock passage for three values of wave Mach number. For low Mach numbers (1.32 and 1.45), only the water surface instabilities are visible with slight spray formation in the recirculation region at the beginning of the water layer (for $M_s = 1.45$). For higher shock Mach number ($M_s = 2.3$) the entire surface of the water is covered with the mist. Figure 9 shows the perturbations on the water surface induced by shocks of low Mach number.

The dependence of the dispersed layer thickness measured at the distance of 90 mm from the beginning of the water layer with time for several values of shock Mach number in the range of $1.6 < M_s < 2.3$ is given in Fig. 10. The results show that the mist thickness grows linearly with time and that the layer thickness only weakly depends on shock Mach number. The artificially introduced capillary waves (ripples) on the water surface increase only the initial growth of the spray layer. A coarse spray is generated for $M_s < 1.5$; a fine spray or mist is generated for $M_s > 1.6$. There are pronounced streamwise disturbances in the mist layer.

4 Discussion

The observations can be divided into two categories—events at early times, up to 500 μs; and events at long times, .5 to 5 ms.

Early time

At early times, 0 to 500 μs, the flow in the present experiment is dominated by the interaction of the shock wave with the water layer. For the shock wave Mach numbers used in the present experiments, the interaction is irregular. The refraction of the shock wave produces a free

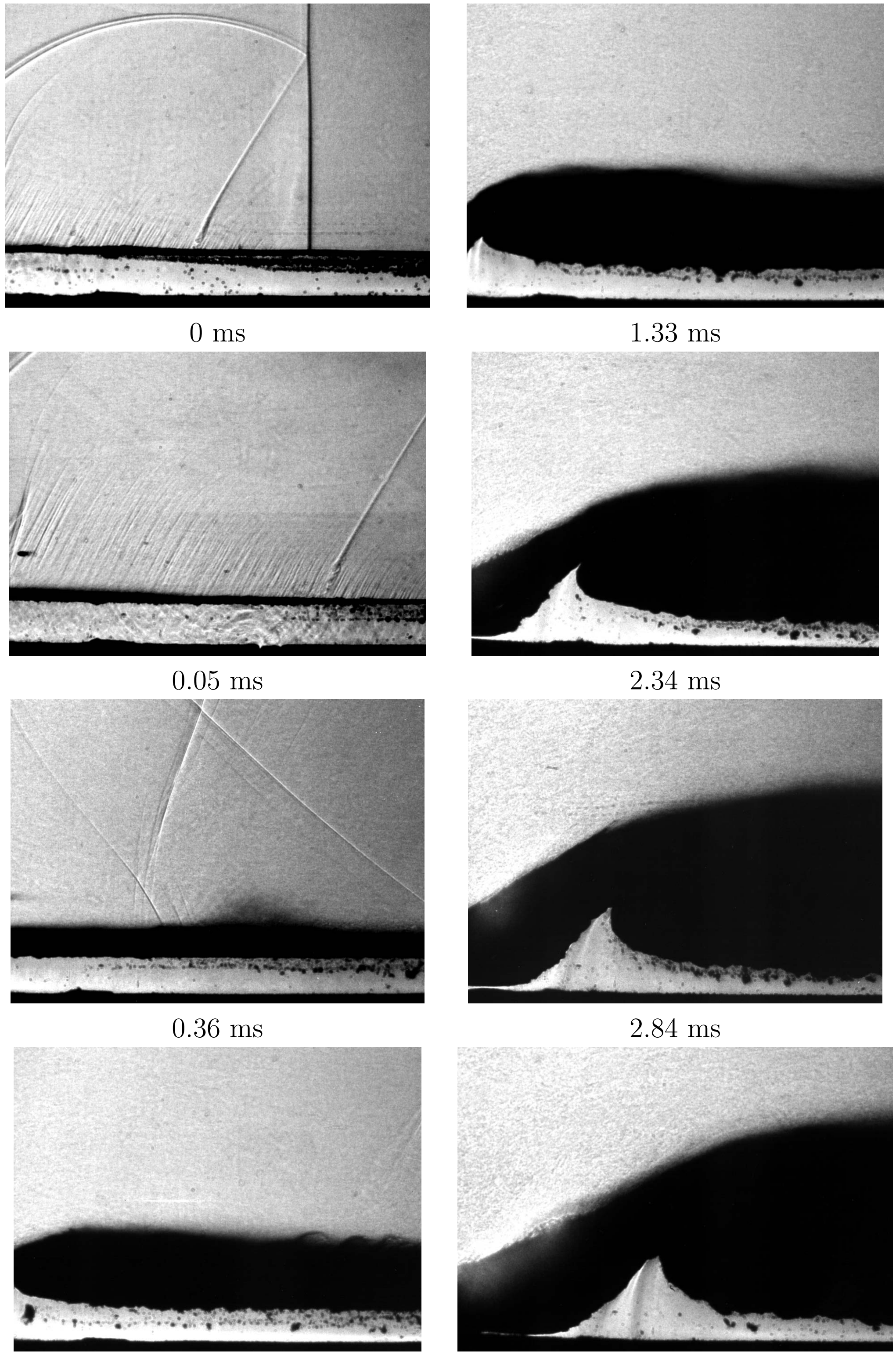

Figure 4: Time sequence of shadow spark photographs of water spray entrainment by shock induced air flow; shock Mach number $M_s = 2.3$.

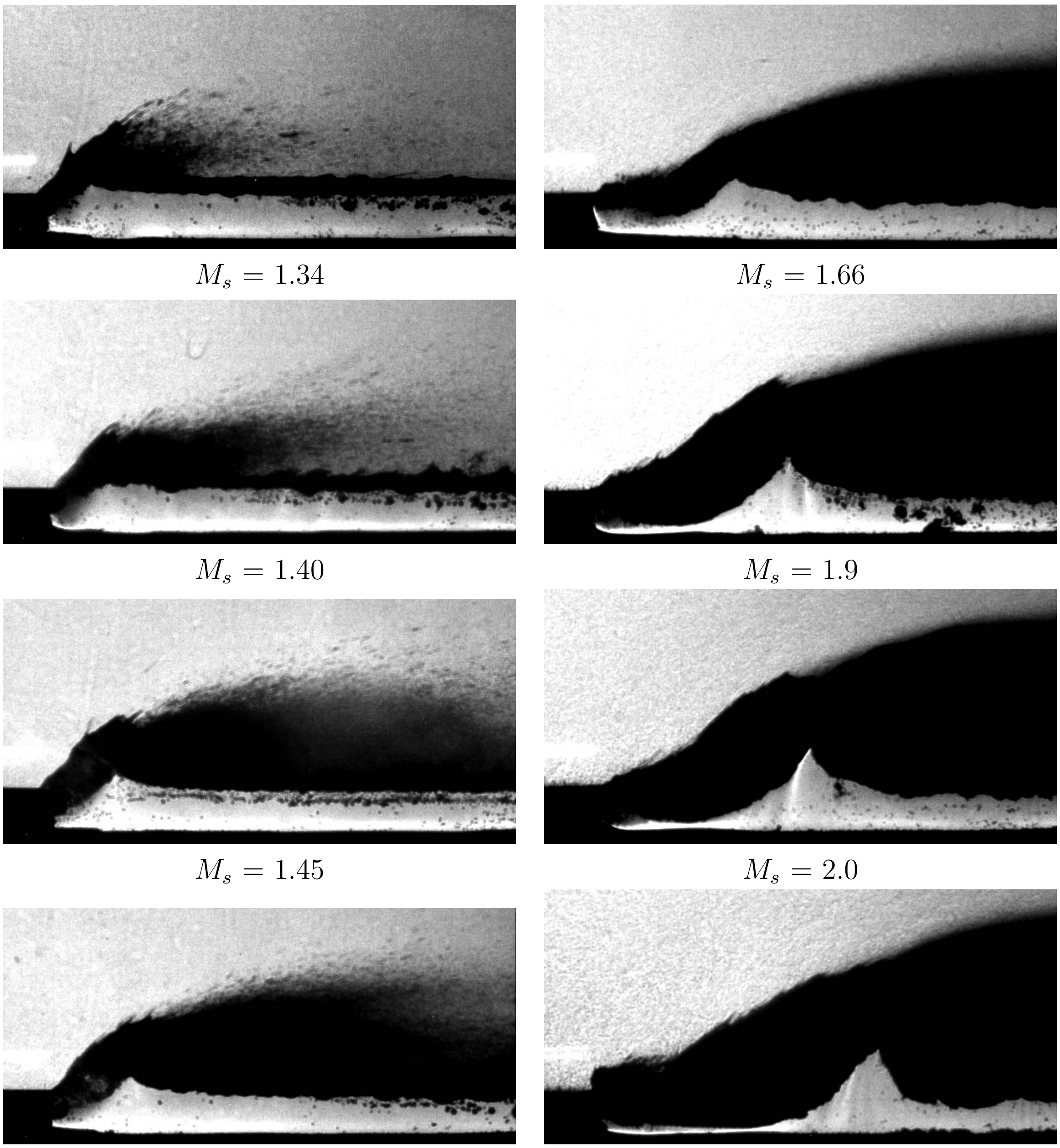

$M_s = 1.34$ $M_s = 1.66$

$M_s = 1.40$ $M_s = 1.9$

$M_s = 1.45$ $M_s = 2.0$

$M_s = 1.51$ $M_s = 2.3$

Figure 5: Shadow spark photographs of water spray entrainment by shock induced air flow at the time 3 ms after shock passage for several values of shock wave Mach number. Surface initially quiescent.

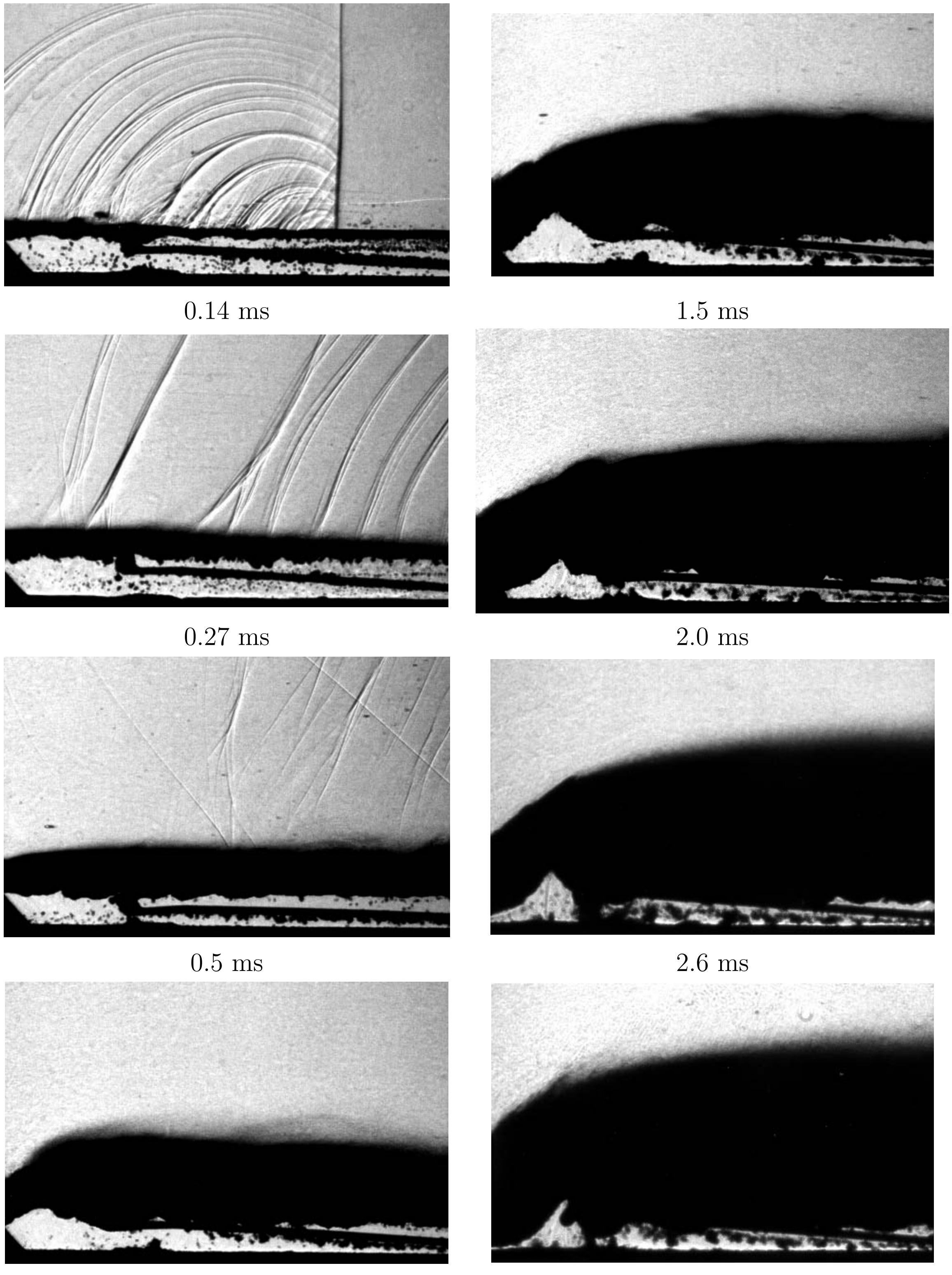

Figure 6: Time sequence of shadow spark photographs of water spray entrainment by shock induced air flow; shock Mach number M = 2.3; Capillary waves generated on the water surface before shock arrival.

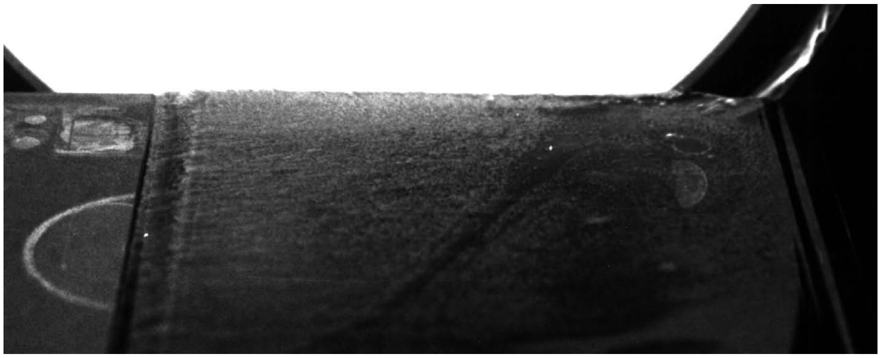

0.2 ms

1 ms

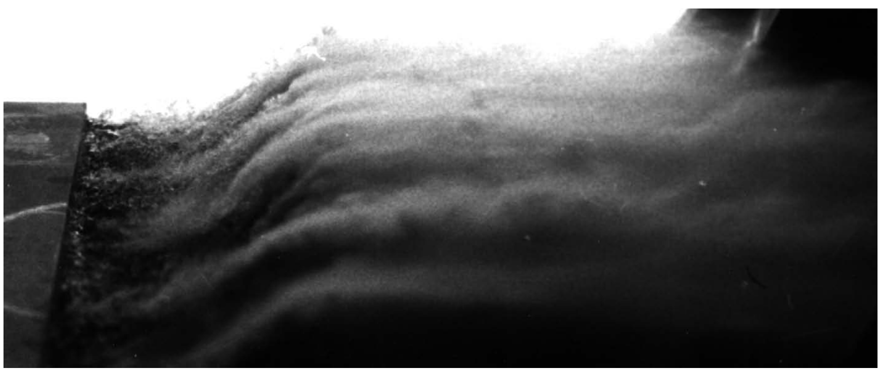

2 ms

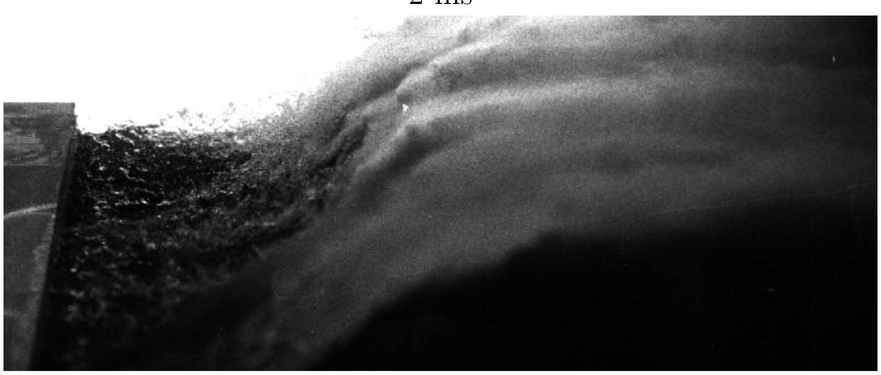

3 ms

Figure 7: Time sequence of direct photographs of the water surface during shock induced air flow; shock Mach number $M_s = 2.3$; flow from left to right; images are taken obliquely to the water surface so appear in perspective distortion.

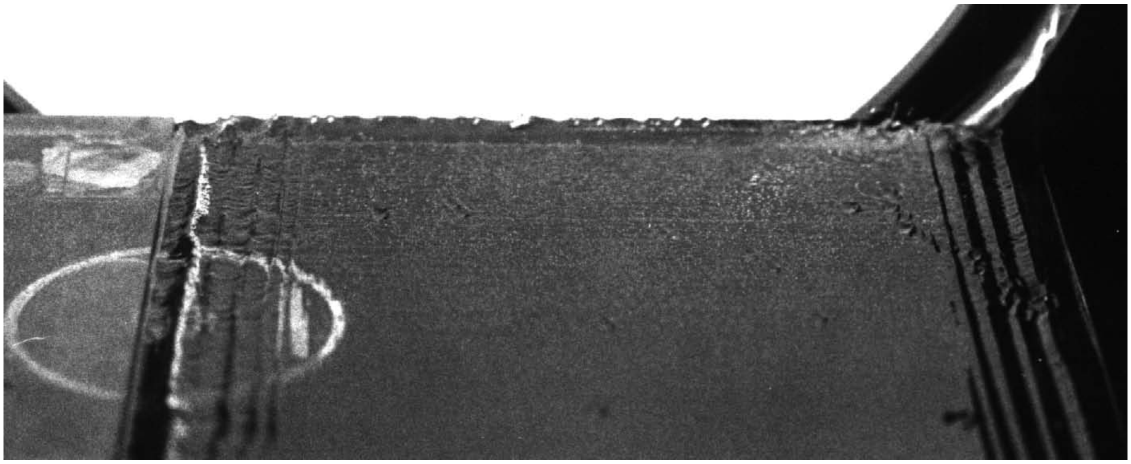

$M_s = 1.32$

$M_s = 1.45$

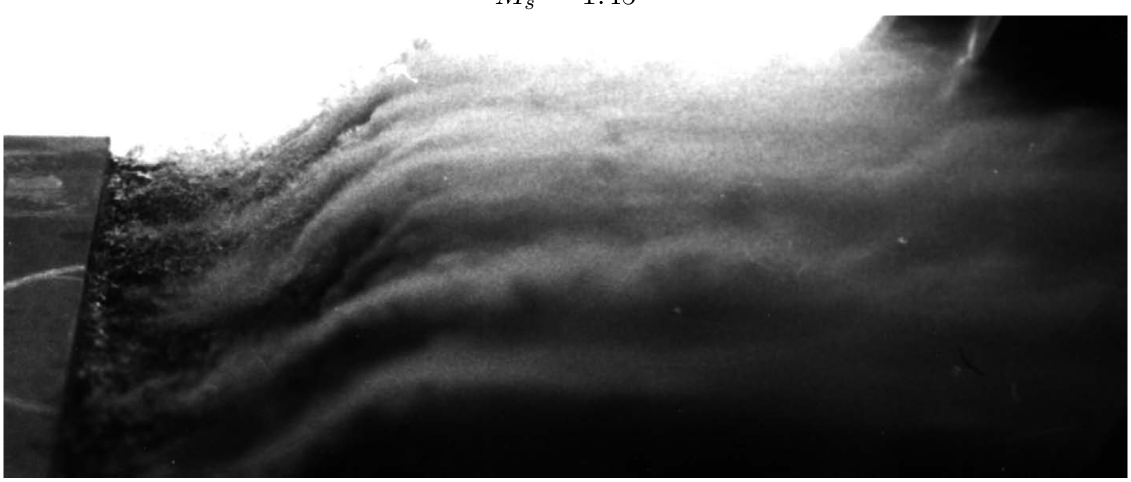

$M_s = 2.3$

Figure 8: Direct photographs of the water surface during shock induced air flow at the time of 2 ms after shock wave passage for three values of shock Mach number. Flow is from left to right, images are taken obliquely to the water surface in perspective distortion.

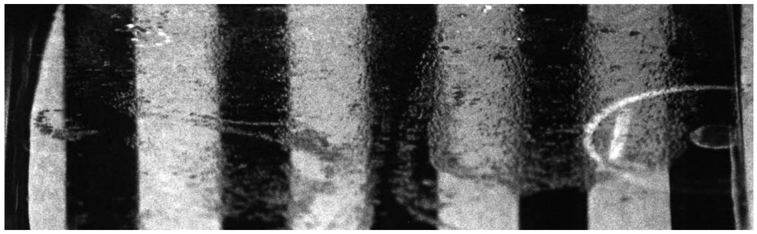

$M_s = 1.2$

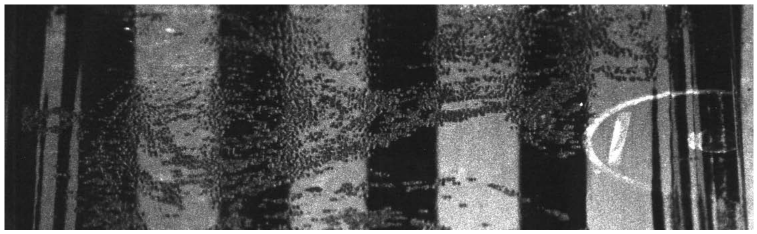

$M_s = 1.25$

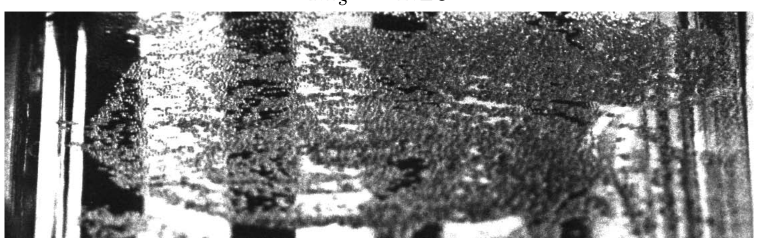

$M_s = 1.35$

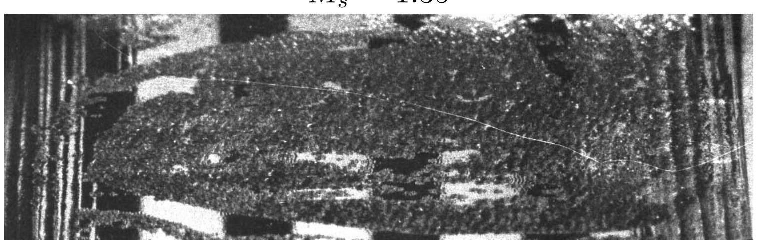

$M_s = 1.4$

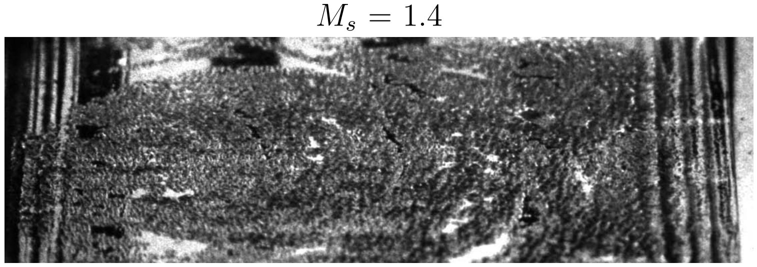

$M_s = 1.45$

Figure 9: Direct photographs of the water surface during shock induced air flow at the time of 0.5 ms after shock wave passage for several low values of shock Mach number $M_s = 1.2$–1.45; flow from right to left; images are taken obliquely to the water surface and are shown in perspective distortion. The black and white bars visible on the bottom of the layer were placed there to aid in flow visualization.

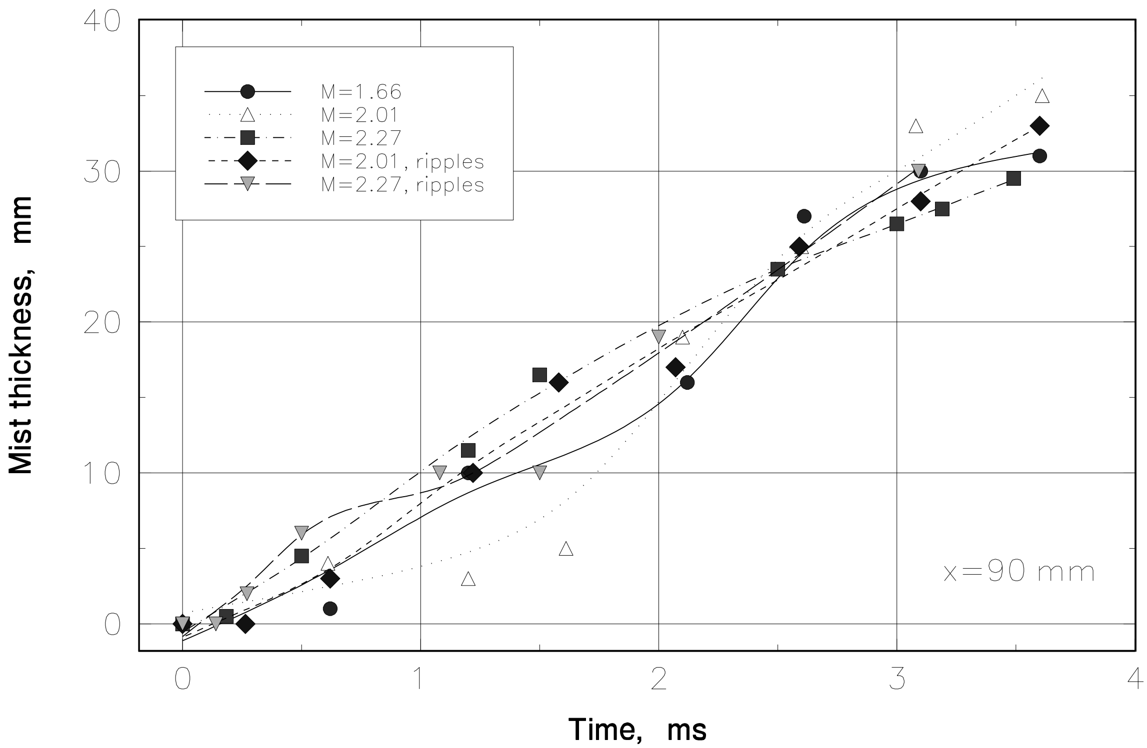

Figure 10: Time dependence of the thickness of mist layer created by shock-induced air flow.

precursor and an evanescent wave in air. The impulsive loading of the water surface by the pressure behind the shock creates ripples on the liquid surface. These ripples spread across the surface and create a broad spectrum of irregular disturbances. The flow over these disturbances generates Mach waves from the free surface.

Ripples on very thin liquid films were observed by Ludwieg and Hornung (1989). In those experiments, an impulsively-started wind tunnel was used to create low-speed flow over an oil-film surface on a flat plate. Nearly transverse ripples with a distinct wavelength were produced under a laminar boundary layer and turbulent "wedges" were observed under a transitional flow. The ripples observed in the present experiment do not have the same appearance and no distinct pattern or wavelength could be observed. The time that the ripples appear in the present experiments appears to be correlated with the onset of turbulent flow in the boundary layer behind the shock wave.

Long time

At longer times, 0.5 to 5 ms, the problem is dominated by a separated flow behind the backward–facing step that forms the upstream boundary of the liquid layer. The acceleration of the water just downstream of the step creates a single traveling wave that moves downstream with an approximately constant velocity. The dispersion of liquid appears to be primarily accomplished by the production of spray from the breaking of the traveling wave. There is a recirculation region downstream of the wave and secondary shock waves due to flow area change created by the solitary wave.

4.1 Traveling Wave Model

A prominent feature of our observations is a steadily-propagating solitary wave. The main features of this wave are outlined in Fig. 11. By carrying out repeated trials at a given shock Mach number, the location of the wave peak can be measured as a function of time from the passage of the initial shock front over the beginning of the liquid layer, see Fig. 12. These experiments indicate that for a Mach 2.3 shock wave, the solitary wave is moving at a velocity $U_w \sim 13$ m/s. This wave is apparently driven by the force resulting from the stagnation of the flow at the end of the recirculation zone just downstream of the step. The wave motion can be analyzed with the help of an approximate momentum equation

$$\frac{d}{dt}\left(MU_w\right) \approx \left(P_t - P_\infty\right)(H-h)w \tag{1}$$

where M is the mass of water in the wave, the wave height $H \sim 3\ h$, and the width of the wave is w. The stagnation pressure P_t - P_∞ can be approximated by $1/2\rho_\infty U_\infty^2$. This gives the following estimate for the wave velocity

$$U_w \approx U_\infty \sqrt{\frac{\rho_\infty}{\rho_{liquid}} \frac{1}{2}\left(\frac{H}{h} - 1\right)} \tag{2}$$

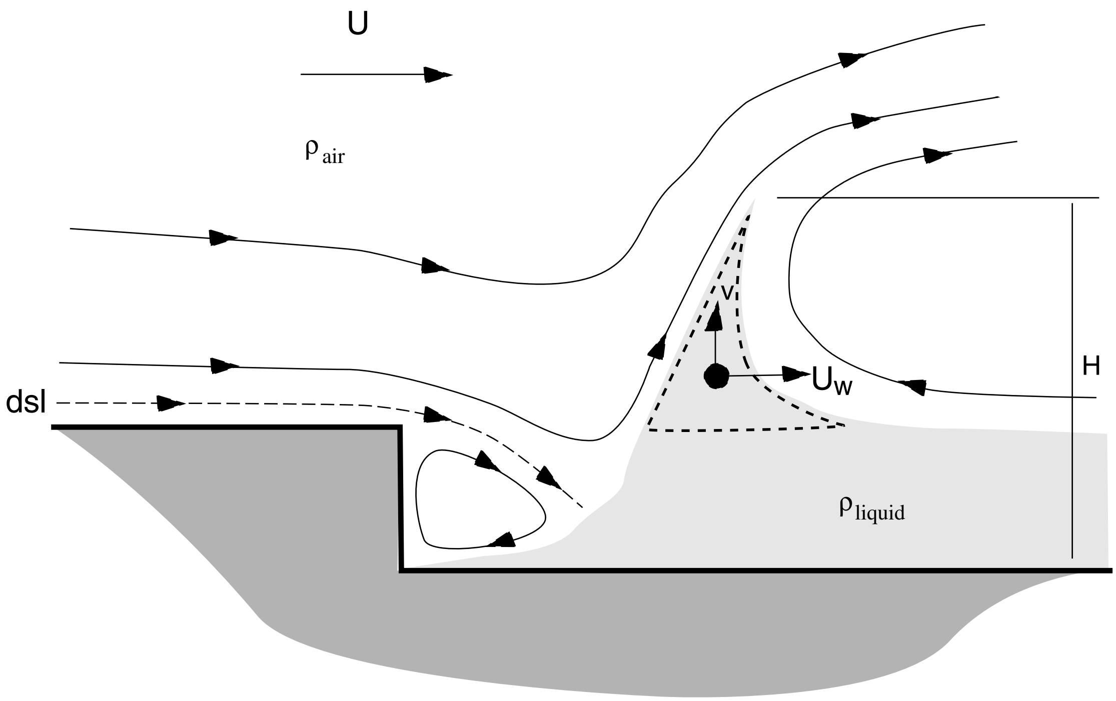

Figure 11: Schematic of flow field in water created by shock-induced air flow.

We have evaluated this for the $M_s = 2.3$ case and computed a wave speed of 15.7 m/s vs a measured speed 13.5 m/s. This agreement indicates that this simple model is reasonable. The vertical pressure gradient in the wave is supported by accelerating fluid

$$P_t - P_\infty \approx \rho_{liquid} H \frac{dv}{dt} \tag{3}$$

which leads to an acceleration $\frac{dv}{dt} \sim 100\ g$.

5 Summary

We have experimentally studied the dispersion of an 8 mm water layer by the flow induced by a shock wave (shock Mach number between 1.4 and 2.4) traveling perpendicular to the nominal free surface. The finite size of the cavity plays a key role in the dispersion mode. Separated flow results in a traveling wave with constant speed that is determined by a momentum balance. The force that drives the wave is apparently generated by the stagnation of the separated flow between the rear-facing step and the wave front. A relatively coarse spray is created for shock Mach numbers less than 1.5 and a fine mist is created for stronger shocks. The refraction of the shock wave from the air to the water appears to play a relatively minor role in comparison with the previous studies on strong (supersonic relative to the liquid layer) shock waves. The surface disturbances begin with a “spotty” surface roughening transition process which may be connected to boundary layer transition to turbulence. Oblique views of the surface show that longitudinal disturbances are visible in the mist layer.

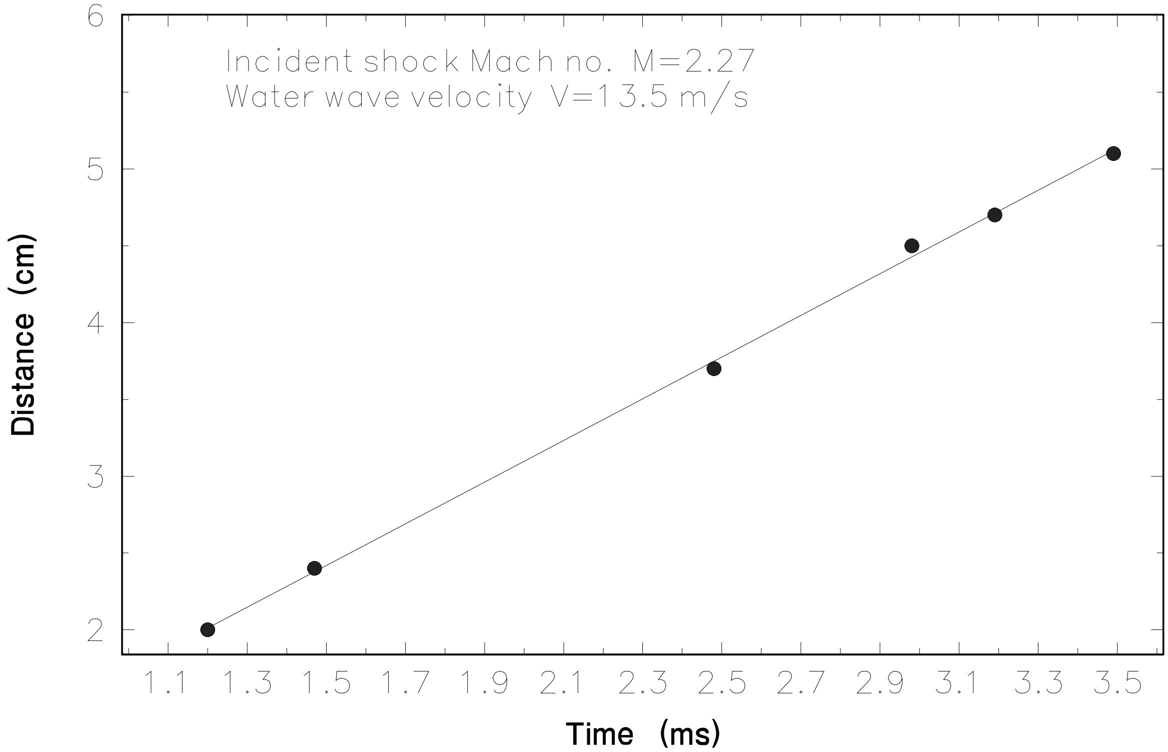

Figure 12: Motion of traveling wave in liquid created by shock-induced air flow.

These may originate from a longitudinal instability of the recirculation region between the rear-facing step and traveling wave. The flow is dominated by the separated region at long times (greater than 0.5 ms) and any model of dispersion in this geometry should take this into account.

6 Acknowledgments

This study was carried out in 1994-1995 when Andrzej Teodorczyk was a Fulbright Fellow visiting Caltech. Preliminary results were presented orally at the 1995 APS meeting (Teodorczyk and Shepherd, 1995).

Bibliography

AA Borisov, SM Kogarko, and AV Lyubimov. Sliding of detonation and shock waves over liquid surfaces. *Combust Explos Shock Waves (USSR)*, 1:19–23, 1965a. 6

AA Borisov, SM Kogarko, and AV Lyubimov. Instability of a liquid surface along which detonation and shock waves are sliding. *Doklady Akademia Nauk SSSR*, 165:125–126, 1965b. 6

AA Borisov, SM Kogarko, and AV Lyubimov AV. Ignition of fuel films behind shock waves in air and oxygen. *Combustion and Flame*, 12:465–468, 1968. 6

AA Borisov, BE Gelfand, SM Sherpanev, and EI Timofeev. Mechanism for mixture formation behind a shock sliding over a fluid surface. *Combust Explos Shock Waves (USSR)*, 17:86–93, 1980. 6

AA Borisov, AH Mailkov, VV Kosenkov, and VS Aksenov. Propagation of gaseous detonations over liquid layers. In *Progress in Astronautics and Aeronautics*, volume 133, pages 268–278. AIAA, 1990. From ICDERS meeting at Ann Arbor in 1989. 6

LF Henderson, J-H Ma, A Skurai, and K Takayama. Refraction of a shock wave at an air-water interface. *Fluid Dynamics Research*, 5:337–350, 1990. 5

S Itaka, J Yang, and K Takayama. Shock propagation over fast/slow and slow/fast interfaces. In R Brun and LZ Dumitrescu, editors, *Shock Waves @ Marseille IB*, pages 293–298. Springer-Verlag, 1989. Proceedings of 19th Symposium on Shock Tubes and Shock Waves. 5

BE Milton, M Behnia, and K Takayama. Interaction of liquid films with shock induced airflows. In K Takayama, editor, *Shock Waves: Proceedings of the 18th Insternational Symposium on Shock Waves*, volume 2, pages 1265–1270. Springer-Verlag, 1992. 6

JA Smith, D Coles, A Roshko, and AJ Prashad. A description of the galcit 6-in shock tube. Technical Report FM-67-1, Graduate Aeronautical Laboratories, California Institute of Technology, 1967. 6

A. Teodorczyk and J. E. Shepherd. Interaction of a shock wave and shock-induced air flow with a water layer. In *Bulletin of the American Physical Society, 48th Annual Meeting of the Division of Fluid Dynamics*, 1995. Abstract II.02. 18

K Yamada, H Nagoya, and K Takayama. Shock wave reflection and propagation over two-liquid interface. In R Brun and LZ Dumitrescu, editors, *Shock Waves @ Marseille II*, pages 299–304. Springer-Verlag, 1995. Proceedings of 19th Symposium on Shock Tubes and Shock Waves. 5

A Shock tube Details

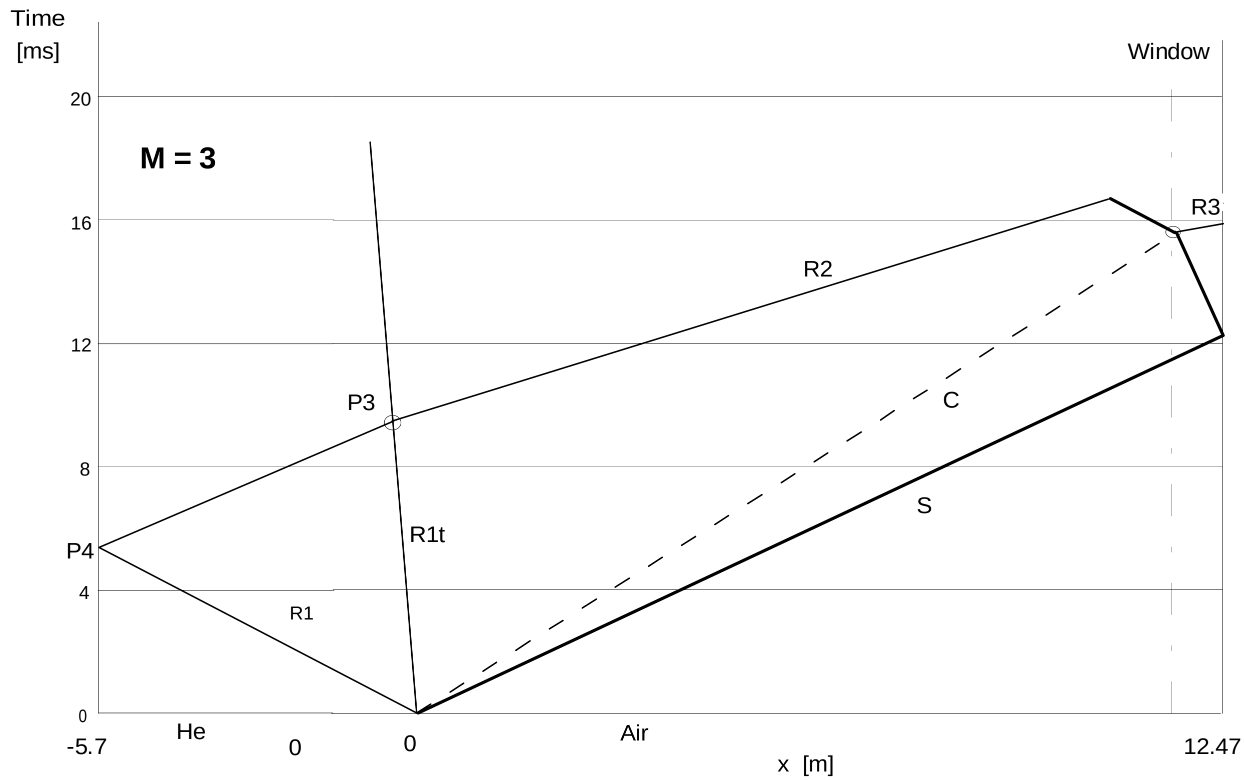

Figure 13: Shock tube performance x-t diagram for $M_s = 3$.

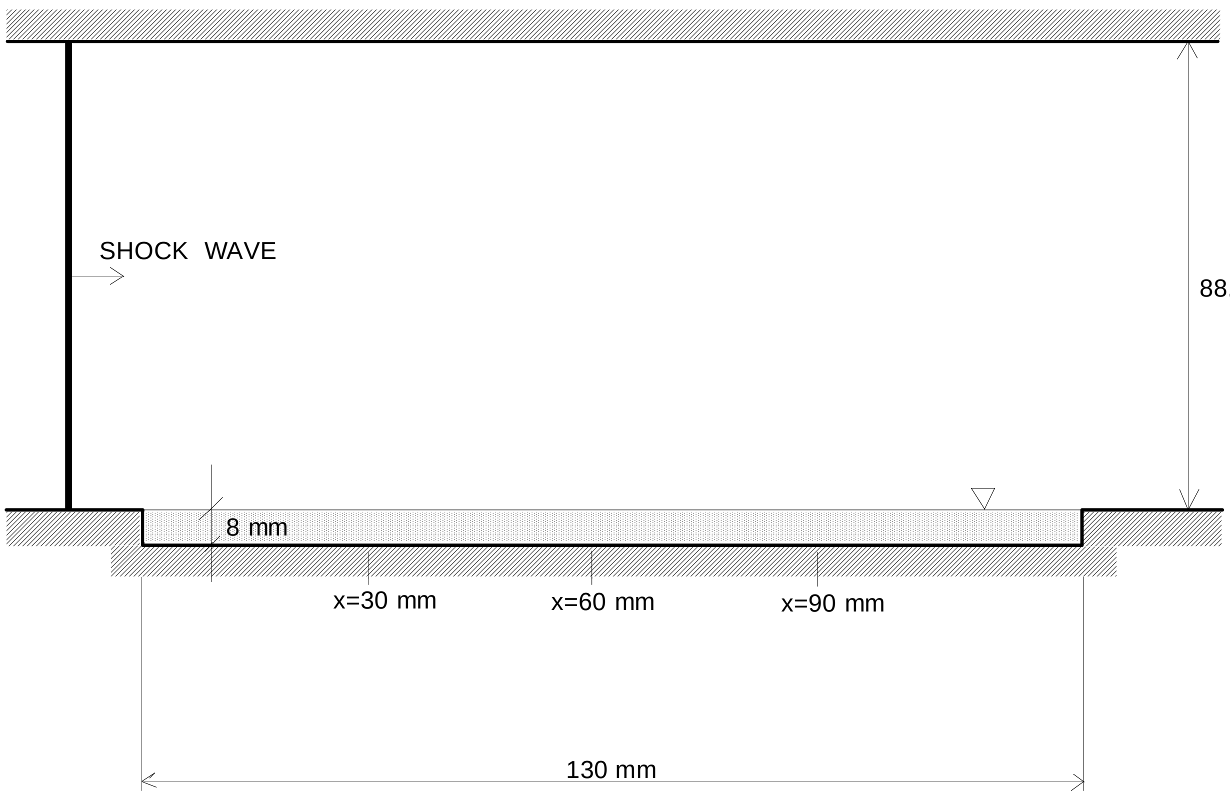

Figure 14: Shock tube test section dimension details.

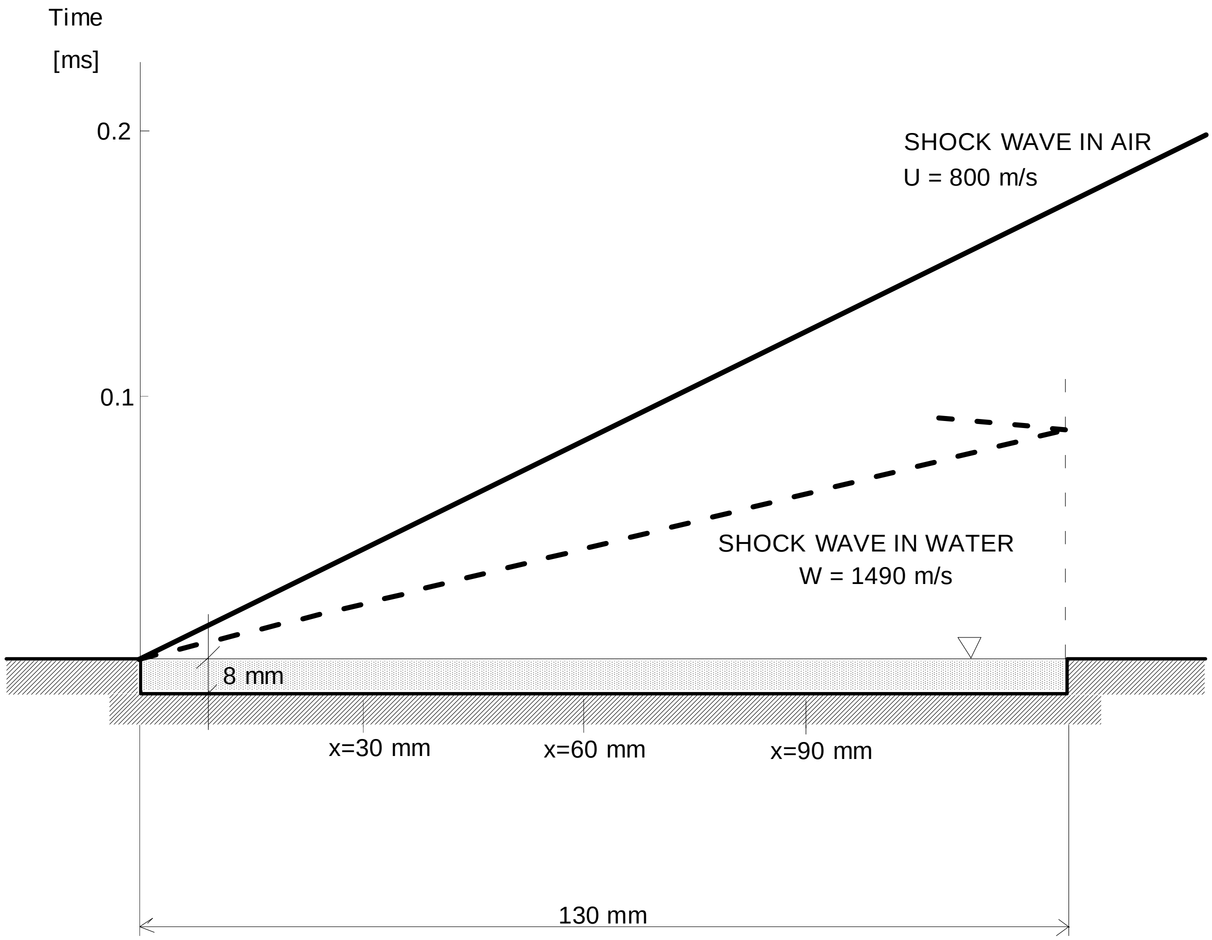

Figure 15: Wave propagation speeds in gas and liquid layers for $M_s = 2.35$.

B Mist Formation

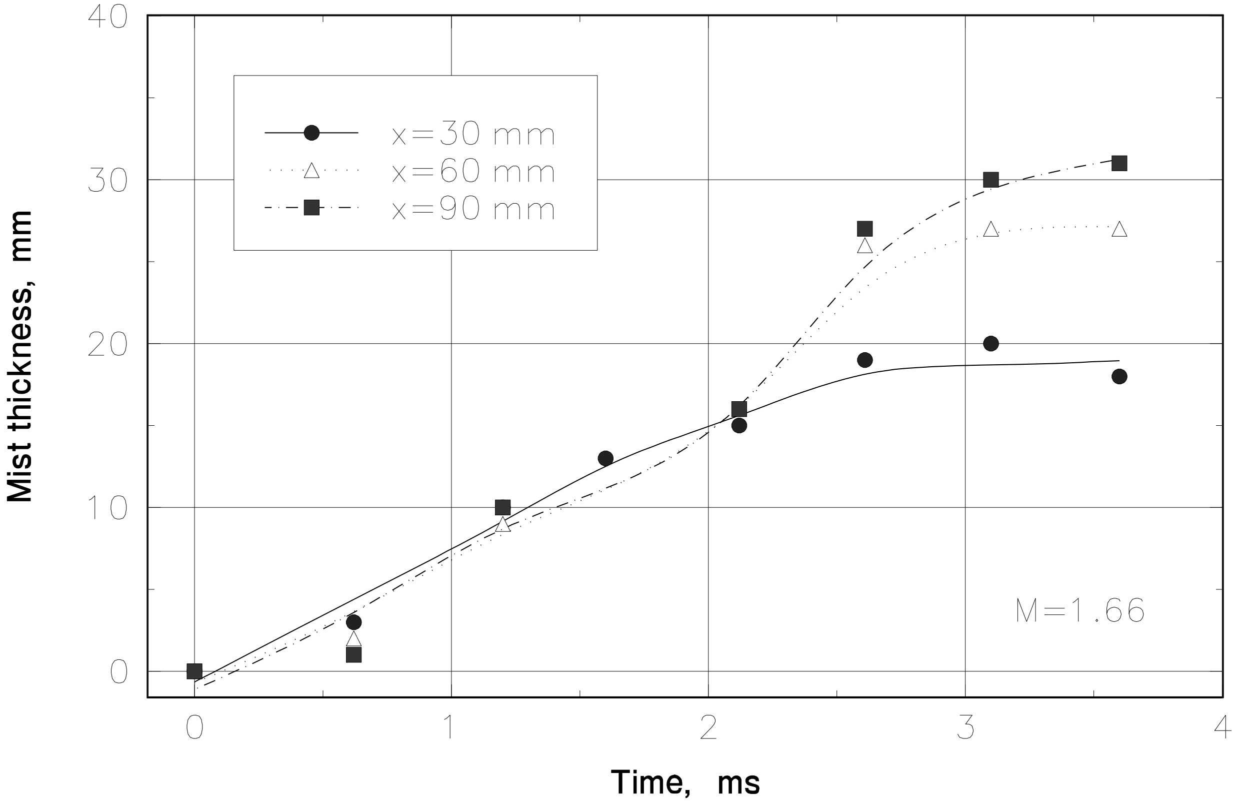

Figure 16: Mist height as a function of time for three locations downstream of the step, M_s = 1.66, initially smooth surface.

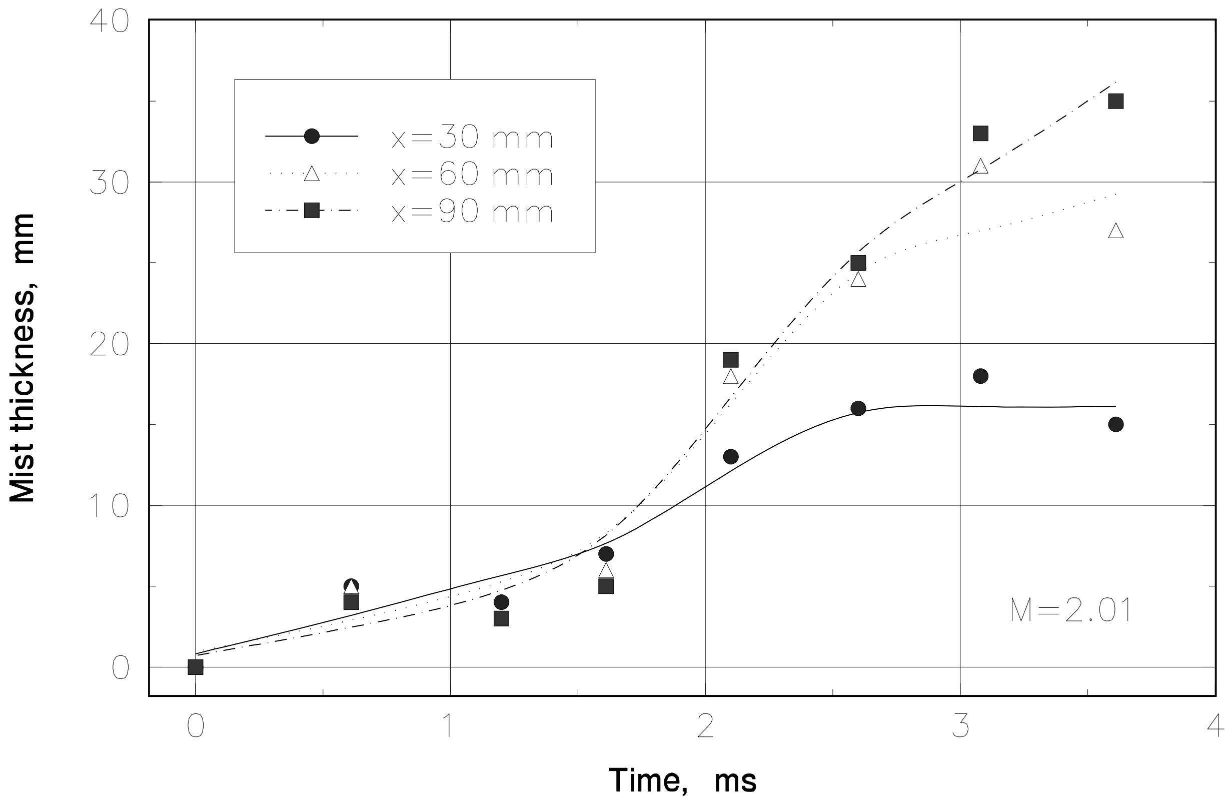

Figure 17: Mist height as a function of time for three locations downstream of the step, M_s = 2.01, initially smooth surface.

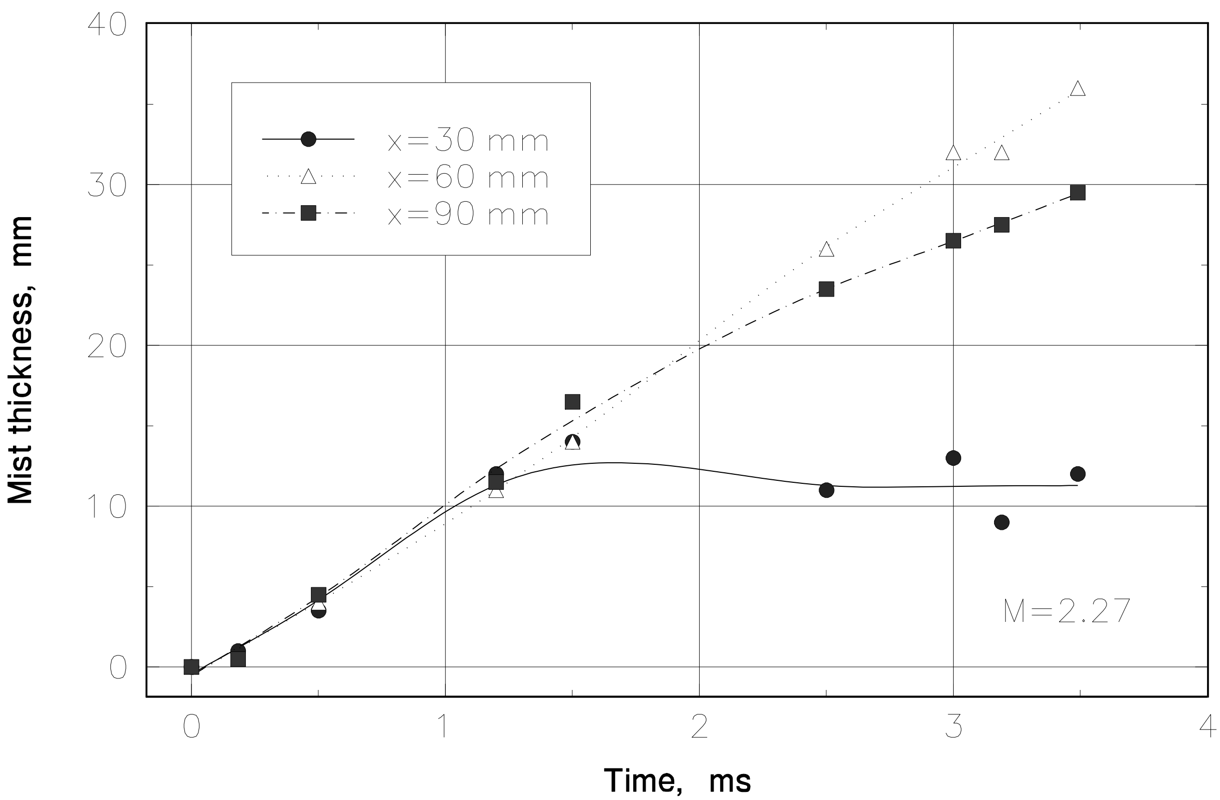

Figure 18: Mist height as a function of time for three locations downstream of the step, M_s = 2.27, initially smooth surface.

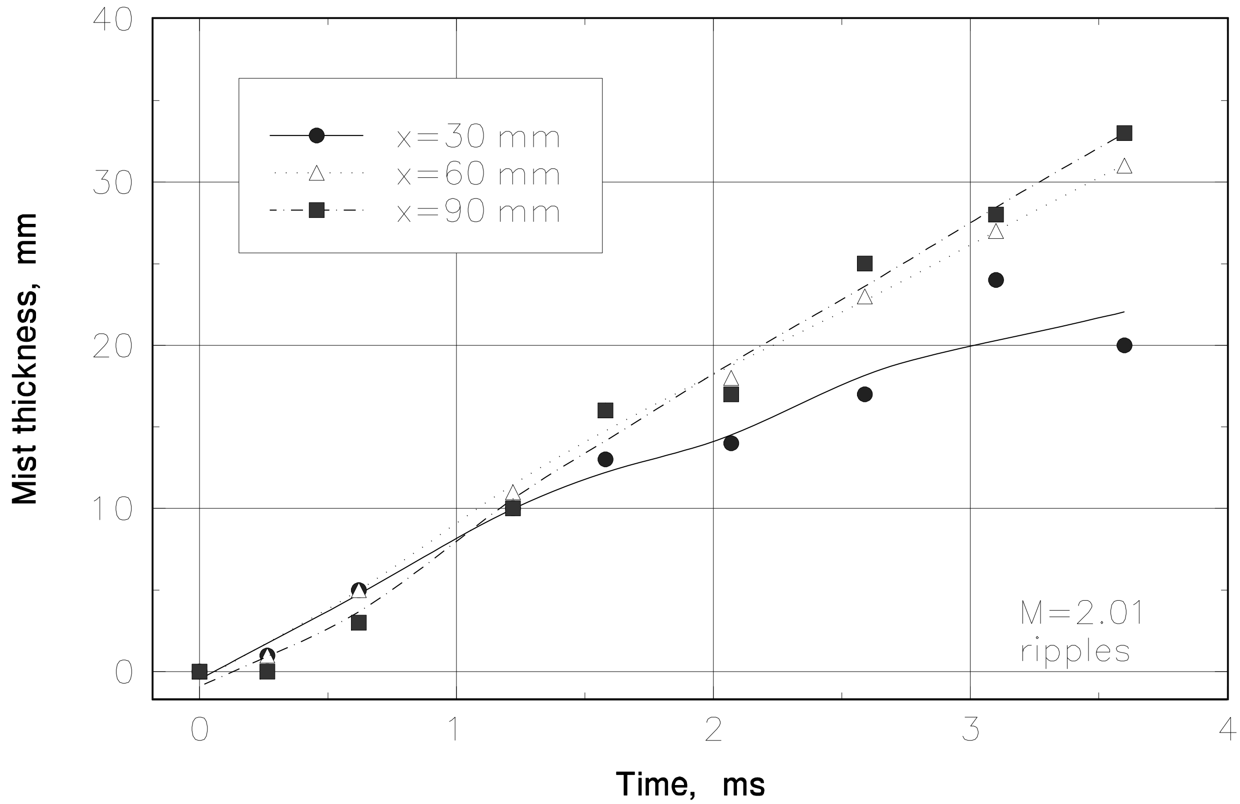

Figure 19: Mist height as a function of time for three locations downstream of the step, M_s = 2.01, initially rippled surface.

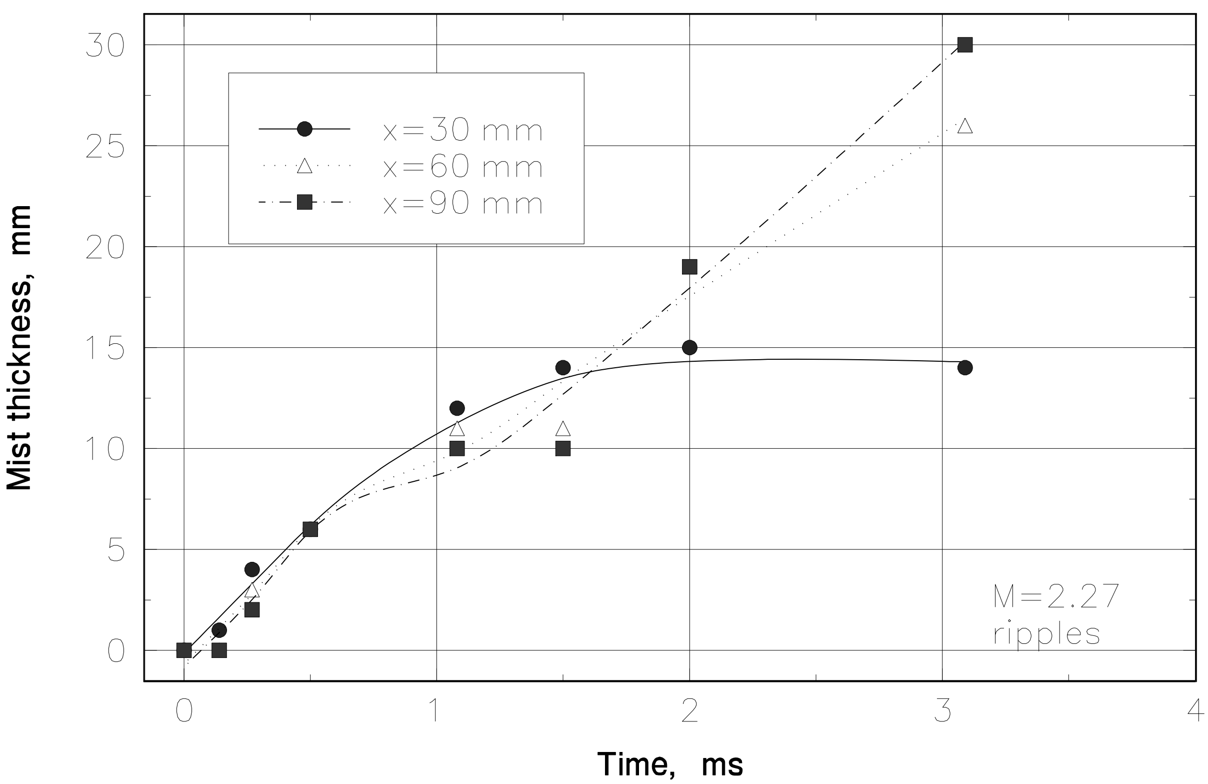

Figure 20: Mist height as a function of time for three locations downstream of the step, M_s = 2.27, initially rippled surface.

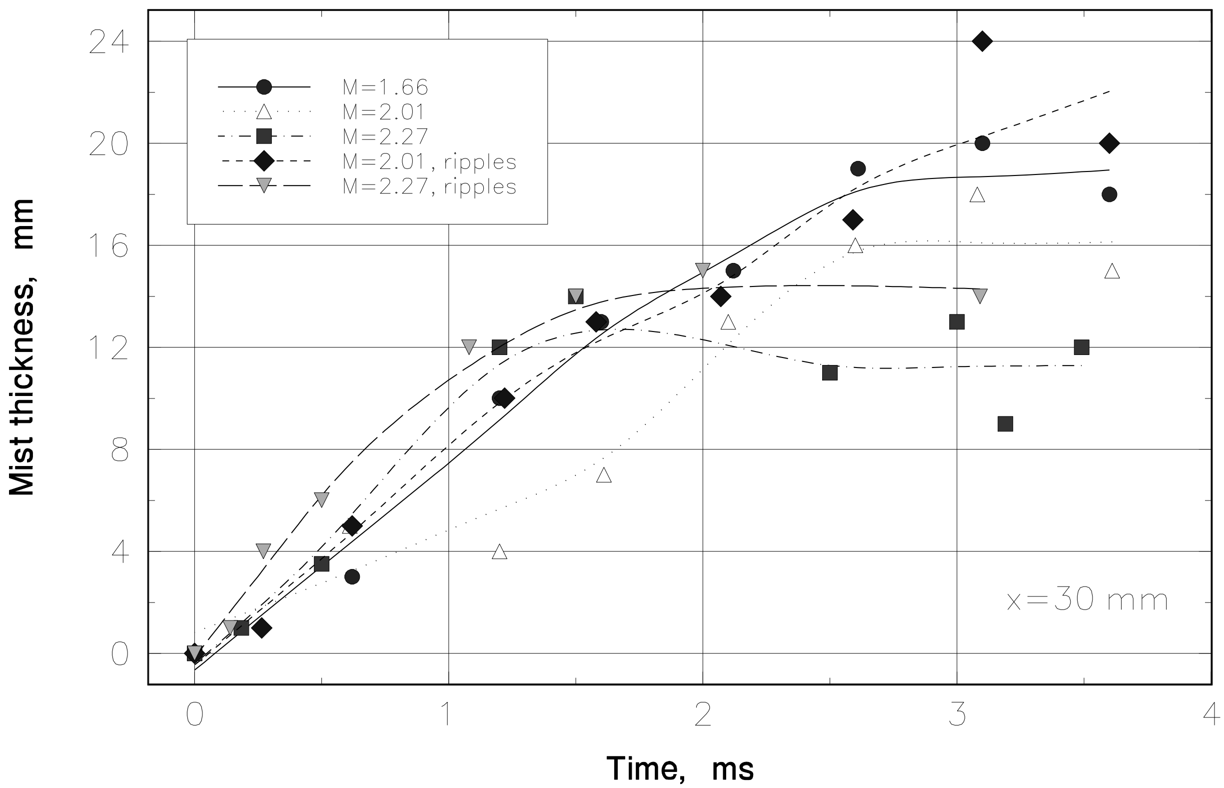

Figure 21: Mist height as a function of time at 30 mm downstream of the step, comparison of five cases.

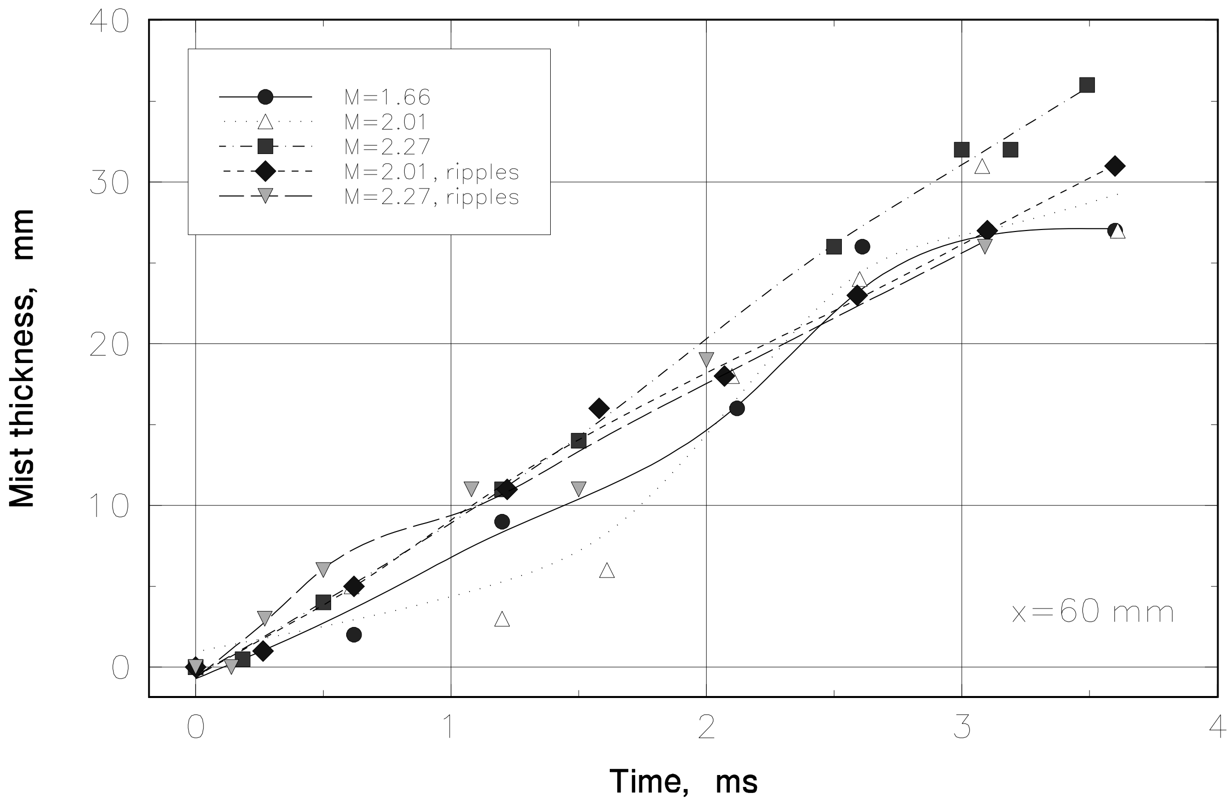

Figure 22: Mist height as a function of time at 60 mm downstream of the step, comparison of five cases.

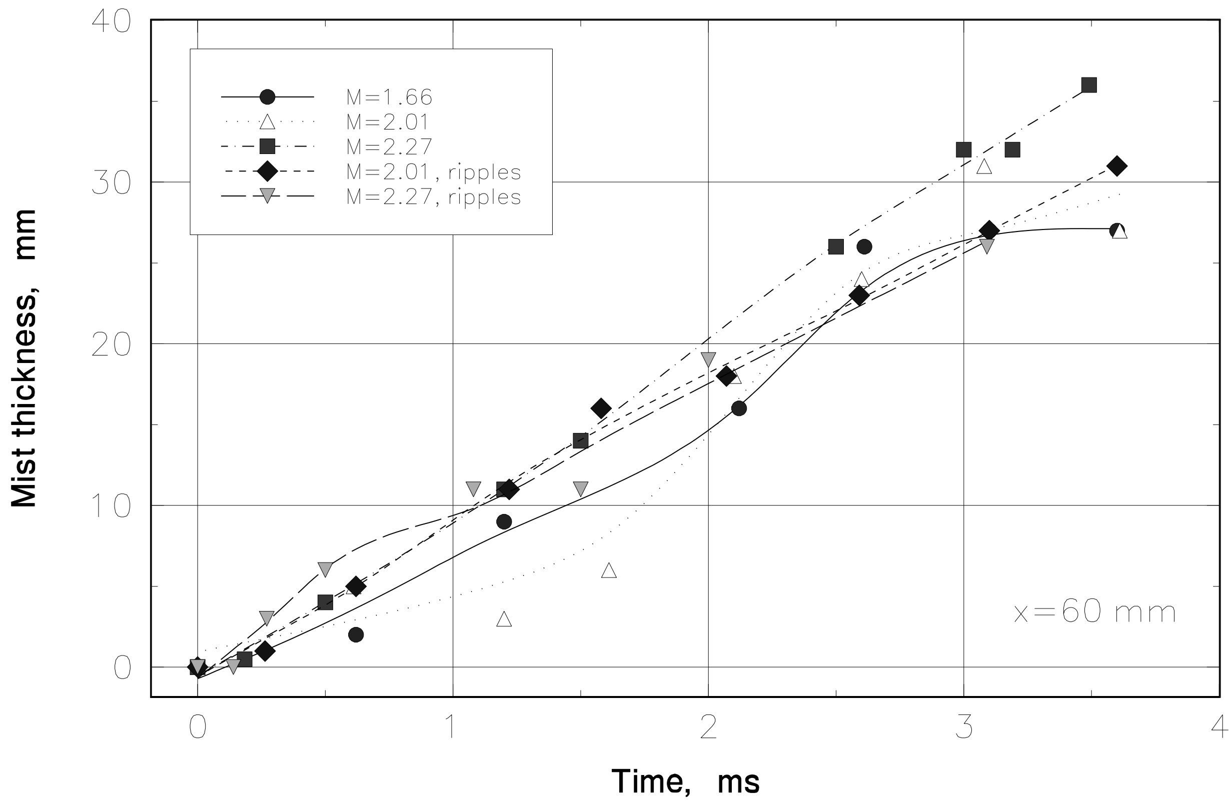

Figure 23: Mist height as a function of time at 90 mm downstream of the step, comparison of five cases.

C Shadowgraph and Perspective Images

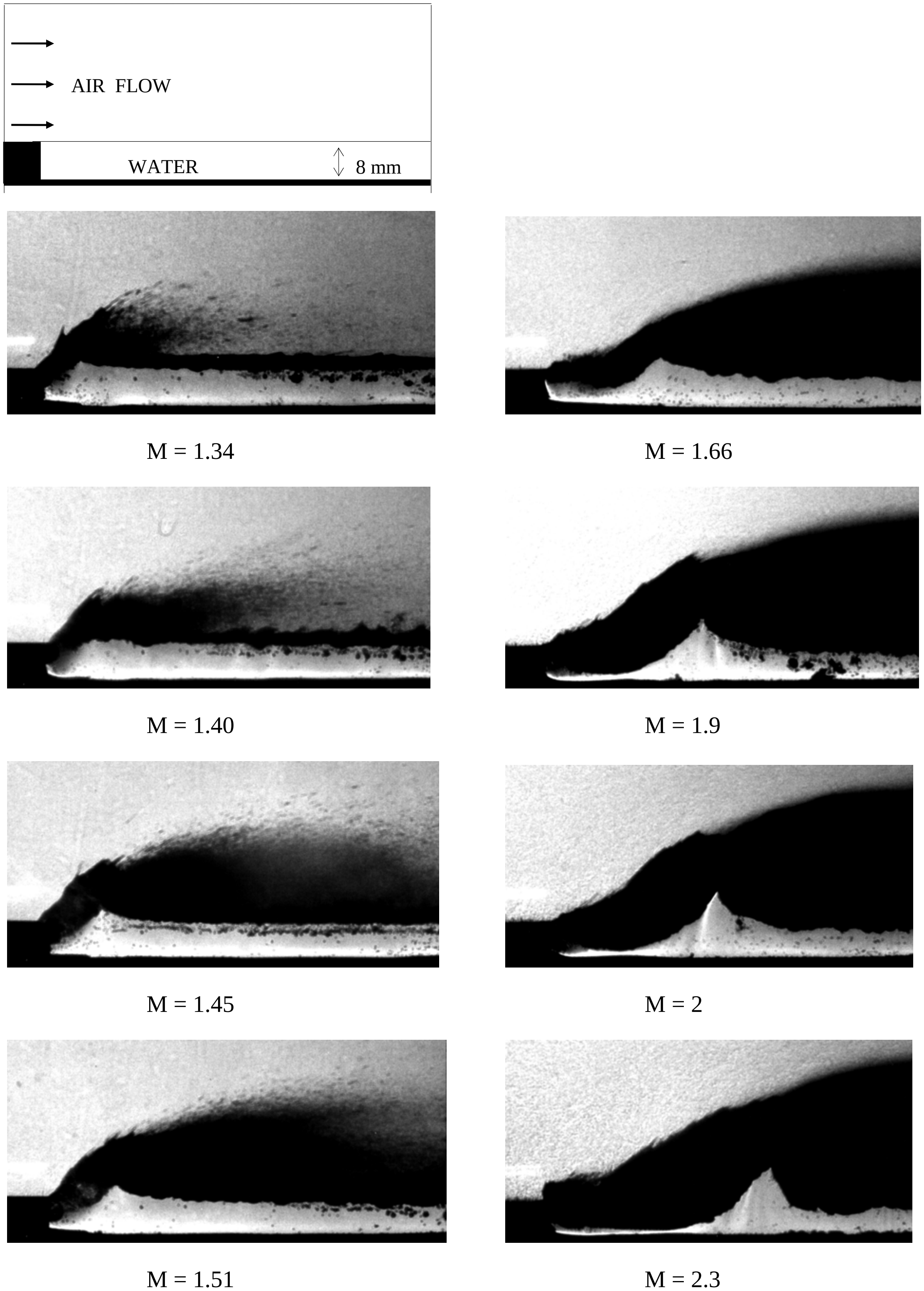

Figure 24: Shadowgraphs at 3 ms after shock passage for $1.34 < M_s < 2.3$, initial pressure 0.25 atm, initially smooth water surface. Air flow is from left to right in these images.

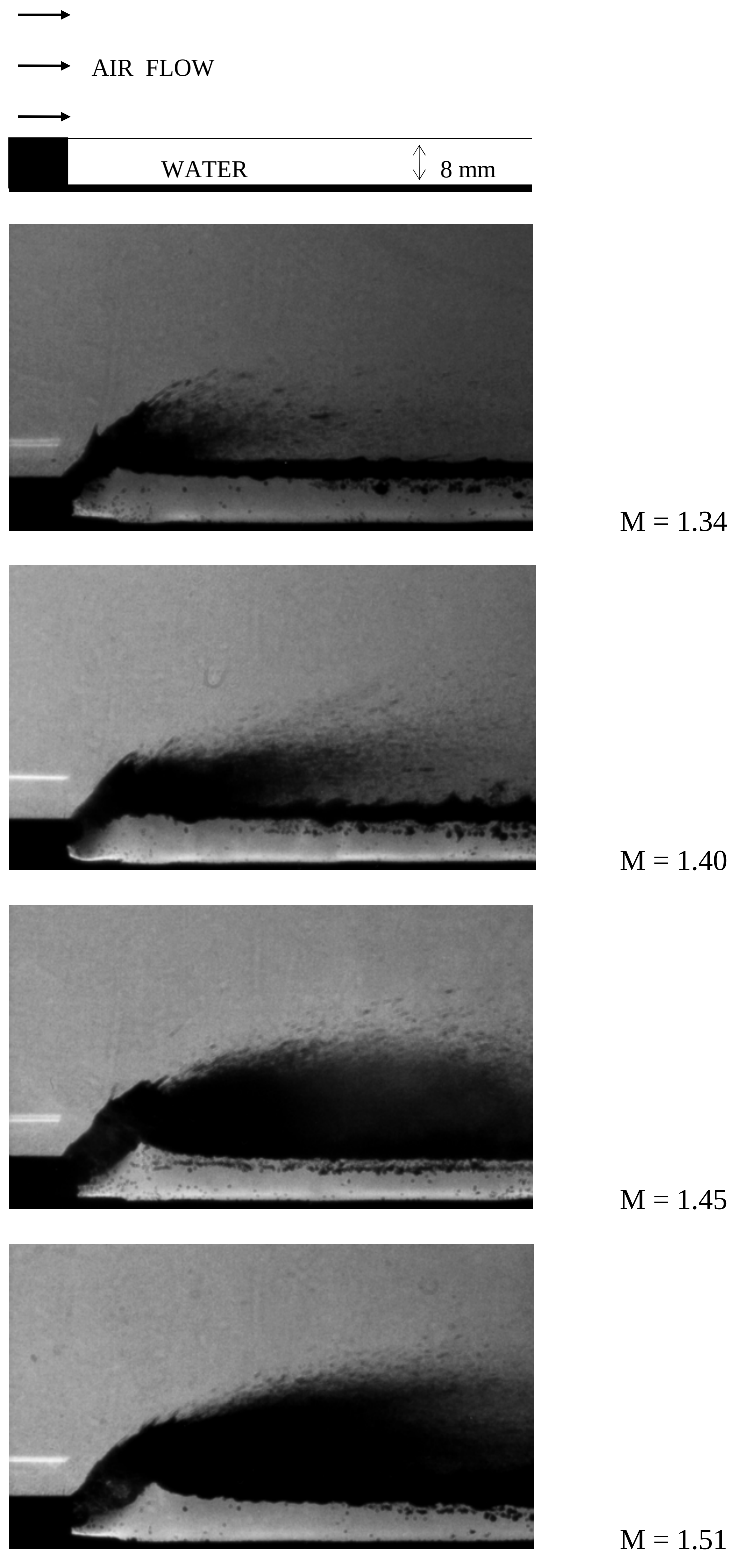

Figure 25: Shadowgraphs showing details of mist formation at 3 ms after shock passage for M_s = 1.34, 1.40, 1.45, 1.51, initial pressure 0.25 atm, initially smooth water surface. Air flow is from left to right in these images.

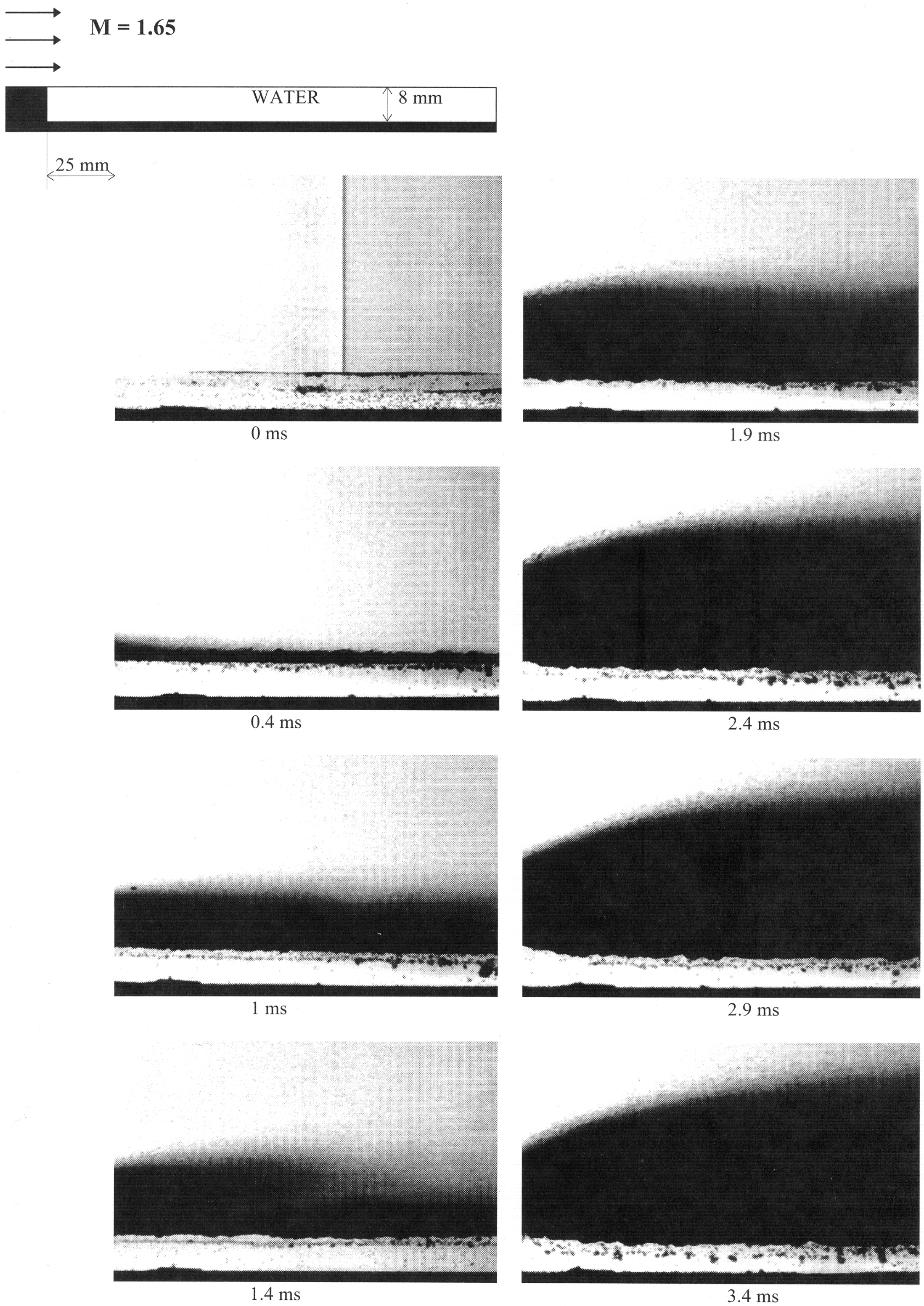

Figure 26: Shadowgraphs showing mist formation as a function of time ($0 < t < 3.4$ ms) after shock passage for $M_s = 1.65$, initial pressure 0.25 atm, initially smooth water surface. Air flow is from left to right in these images.

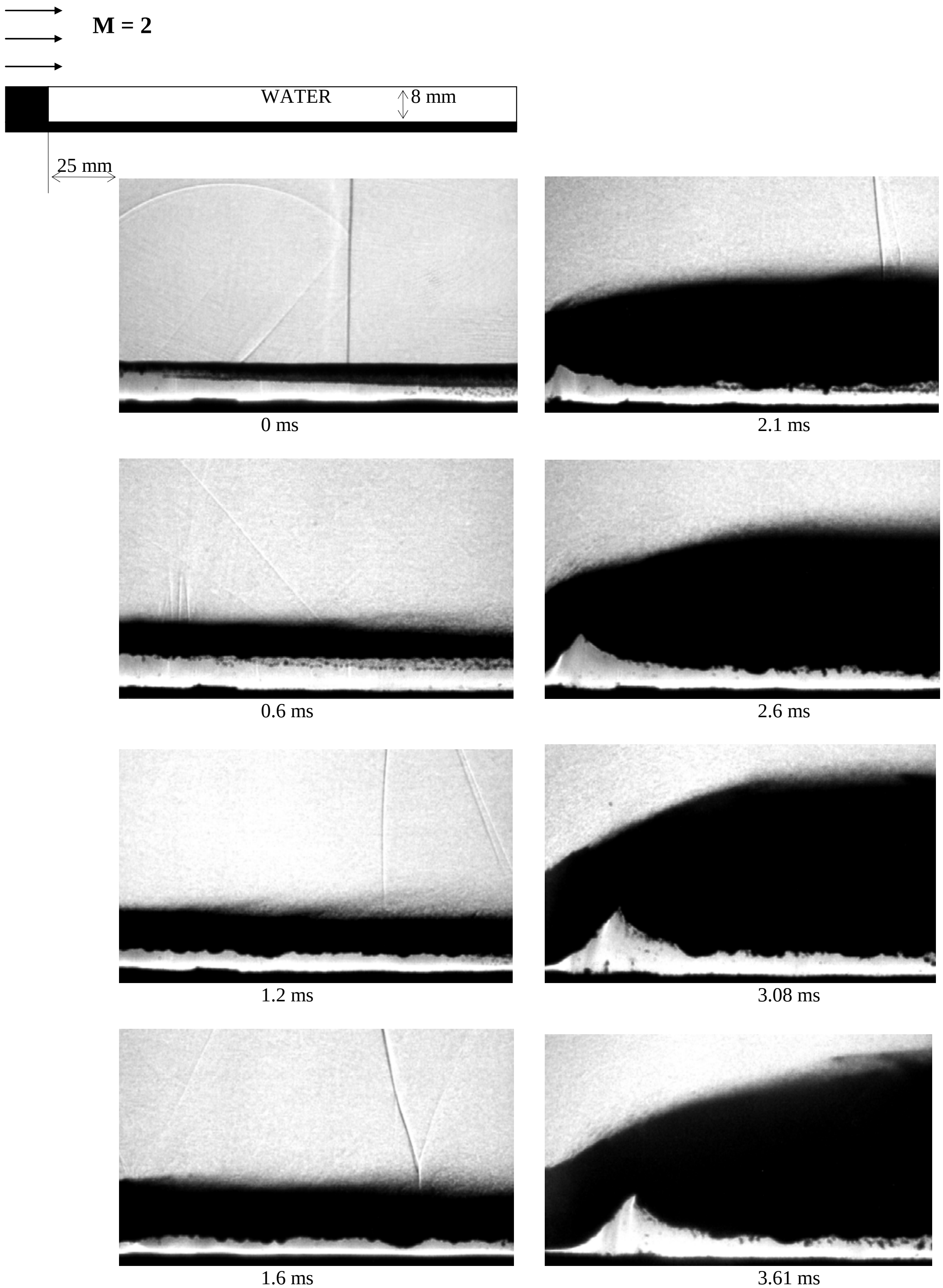

Figure 27: Shadowgraphs showing mist formation as a function of time ($0 < t < 3.61$ ms) after shock passage for $M_s = 2.0$, initial pressure 0.25 atm, initially smooth water surface. Air flow is from left to right in these images.

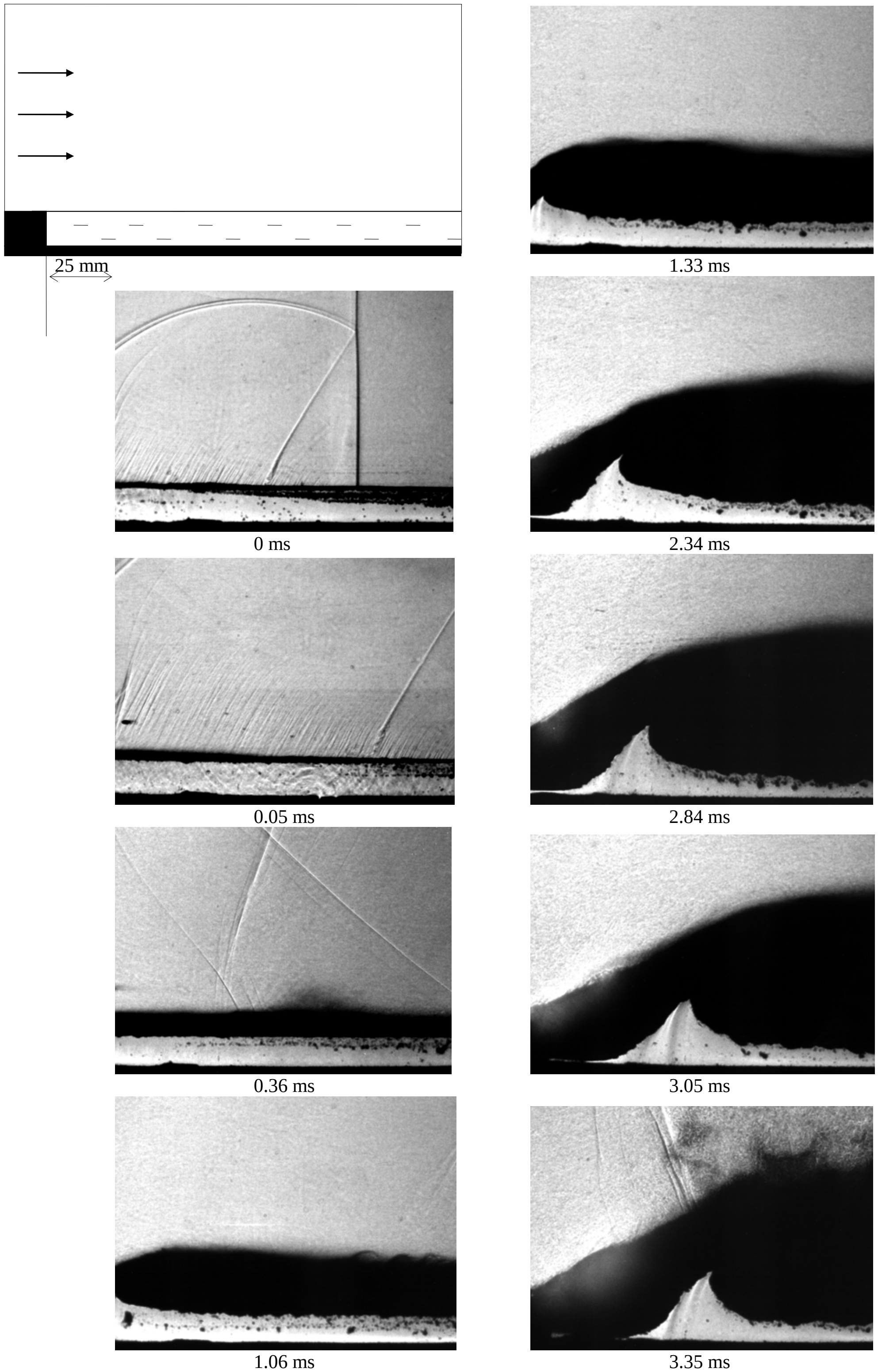

Figure 28: Shadowgraphs showing mist formation as a function of time ($0 < t < 3.35$ ms) after shock passage for $M_s = 2.3$, initial pressure 0.25 atm, initially smooth water surface. Air flow is from left to right in these images.

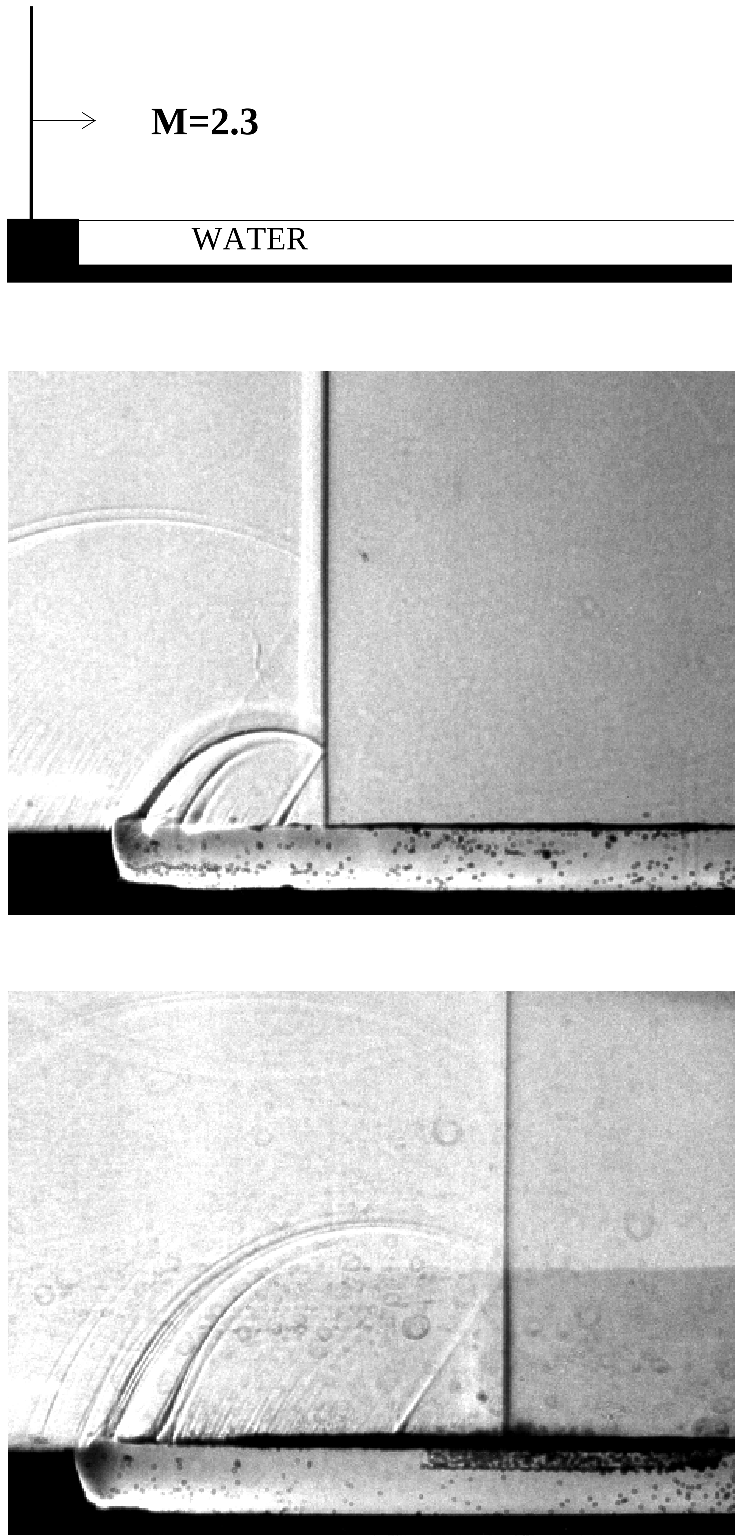

Figure 29: Shadowgraphs showing initial shock wave propagation along water surface, M_s = 2.3, initial pressure 0.25 atm, initially smooth water surface. Air flow is from left to right in these images.

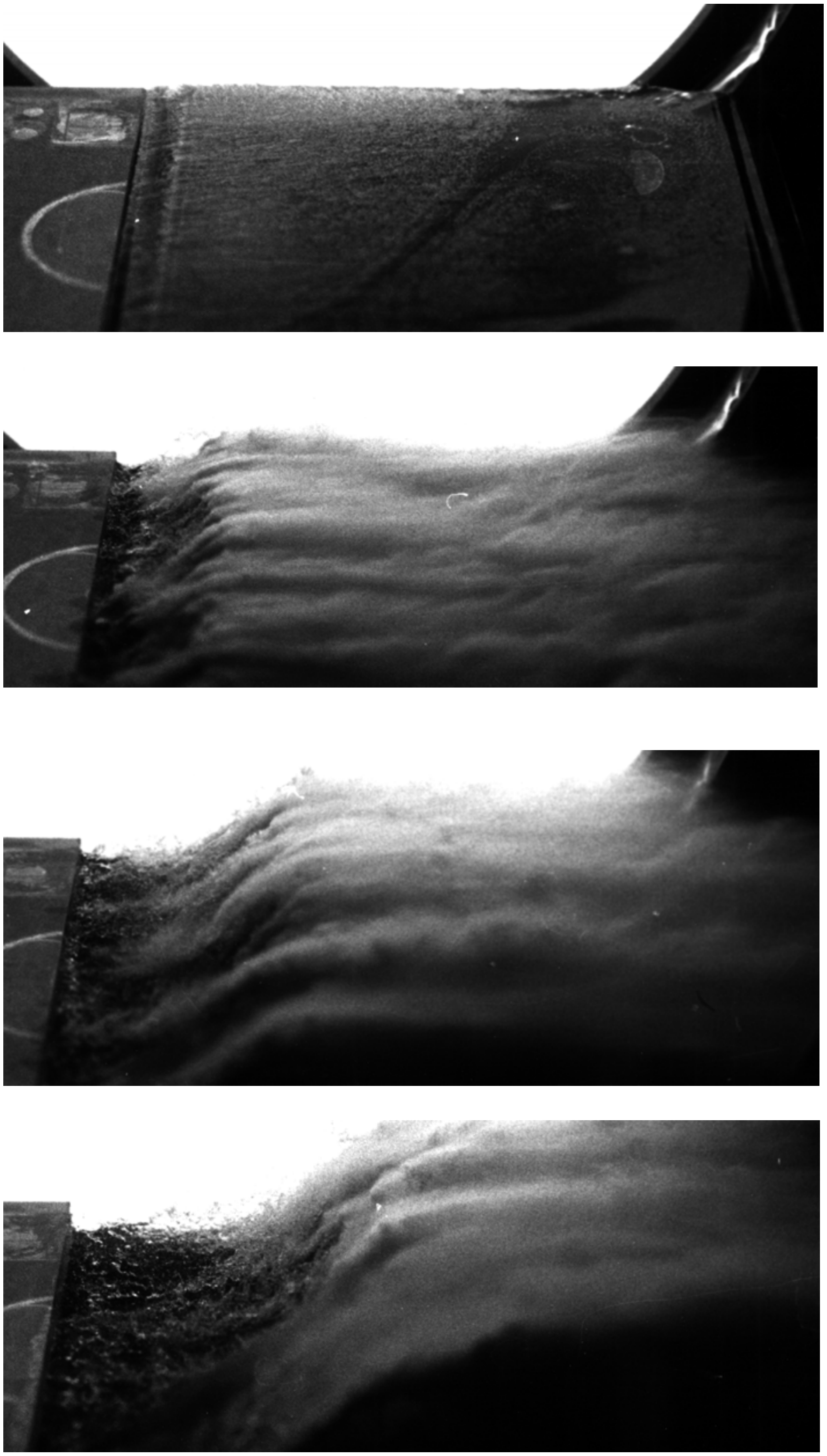

t=0.2 ms

t=1 ms

t=2 ms

t=3 ms

Figure 30: Direct photographs with oblique view showing mist and wave development on water surface, $M_s = 2.3$, initial pressure 0.25 atm, initially smooth water surface. Air flow is from left to right in these images.

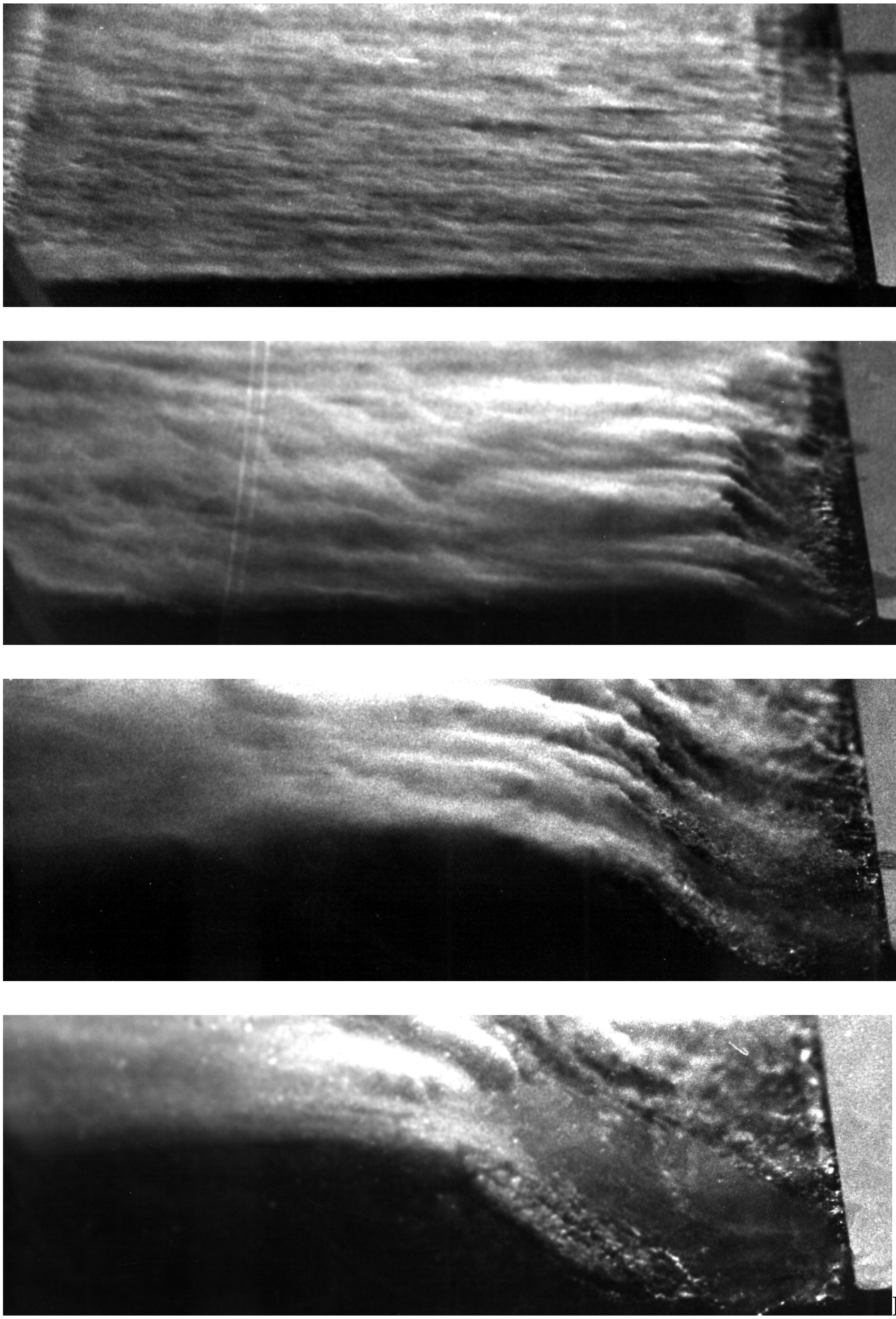

M = 2.3; t = 0.5 ms

M = 2.3; t = 1 ms

M = 2.3; t = 2 ms

M = 2.3; t = 3 ms

Figure 31: Direct photographs with oblique view showing close up view of mist and wave development on water surface, $M_s = 2.3$, initial pressure 0.25 atm, initially smooth water surface. Flow is right to left in these images.

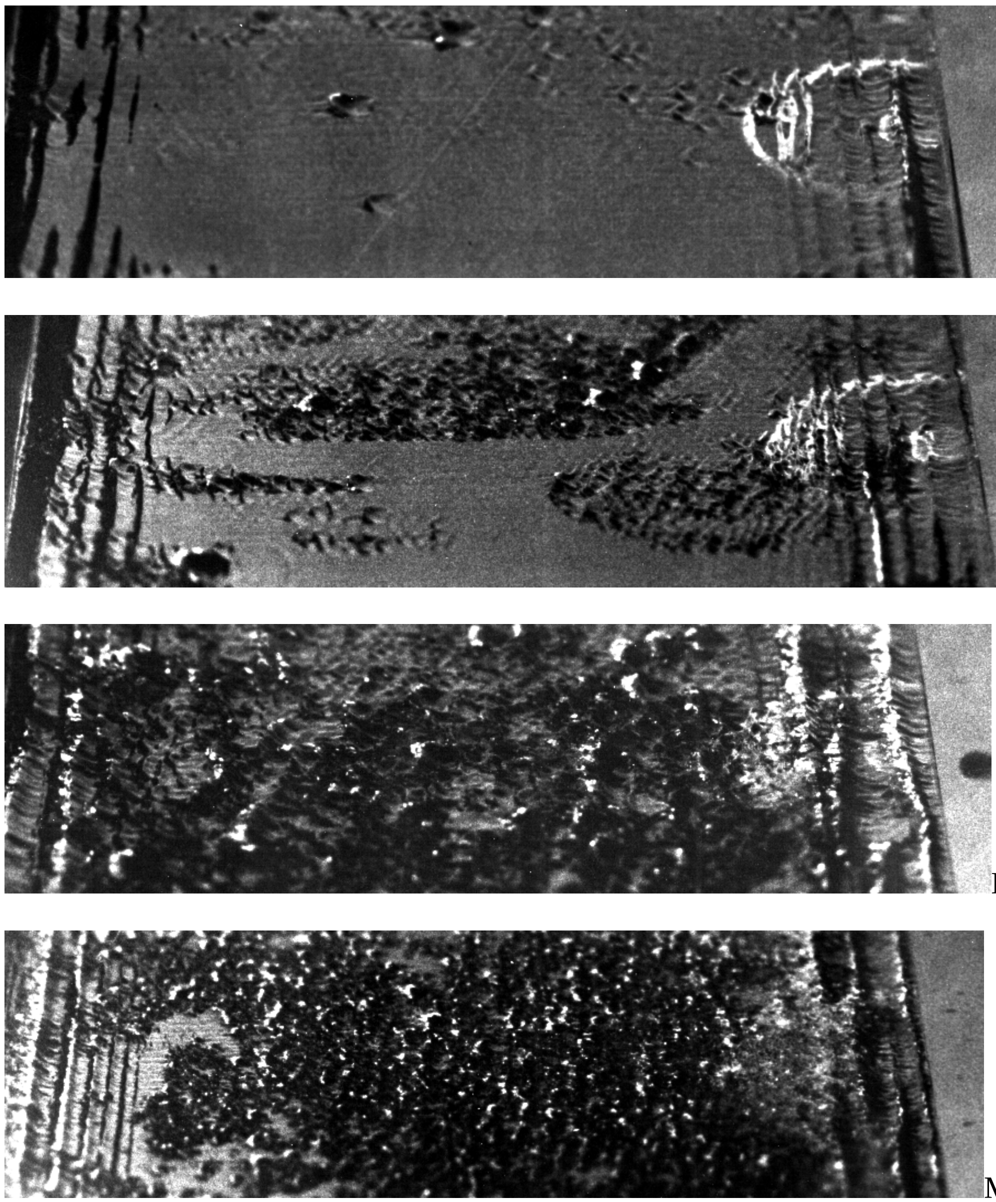

M = 1.25; t = 3 ms

M = 1.30; t = 2 ms

M = 1.40; t = 3 ms

M = 1.51; t = 1 ms

Figure 32: Direct photographs with oblique view showing onset of disturbances on water surface at 1, 2 and 3 ms, M_s = 1.25, 1.30, 1.40, 1.51; initial pressure 0.25 atm, initially smooth water surface. Flow is right to left in these images.

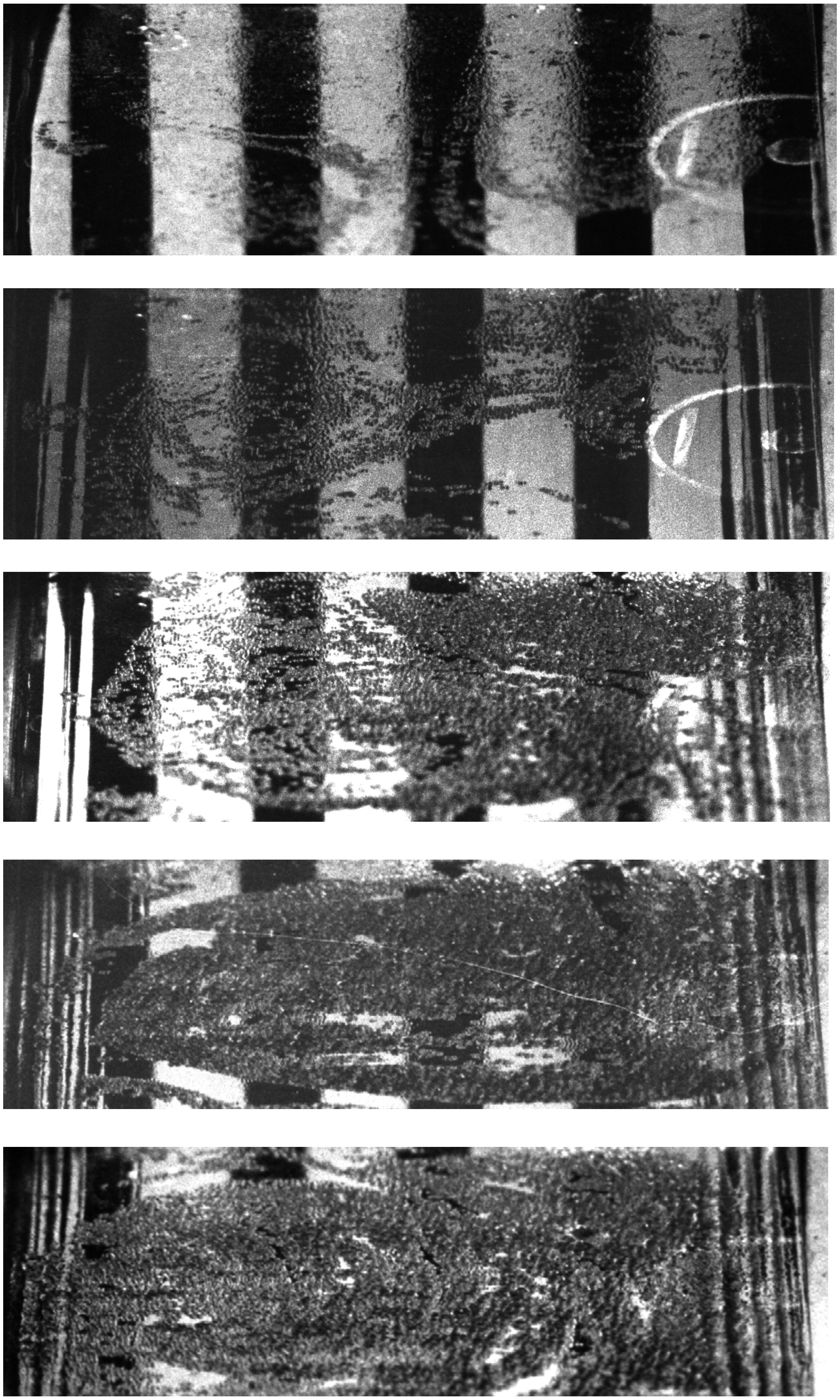

M = 1.2

M = 1.25

M = 1.35

M=1.4

M=1.45

Figure 33: Direct photographs with oblique view showing disturbance on water surface at 0.5 ms after shock wave reaches the cavity., M_s = 1.2, 1.25, 1.35, 1.4, 1.45; initial pressure 0.25 atm, initially smooth water surface. Flow is right to left in these images.

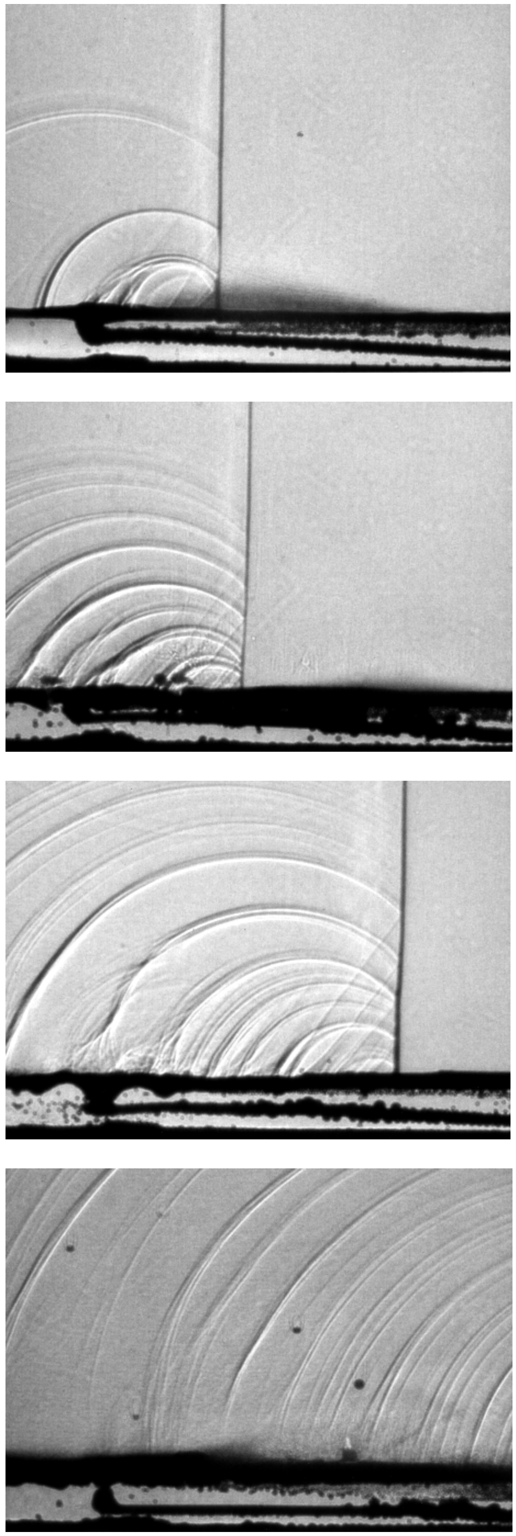

Figure 34: Shadowgraphs showing initial shock wave propagation along water surface, M_s = 2.3, initial pressure 0.25 atm, initially rippled water surface. Air flow is from left to right in these images.

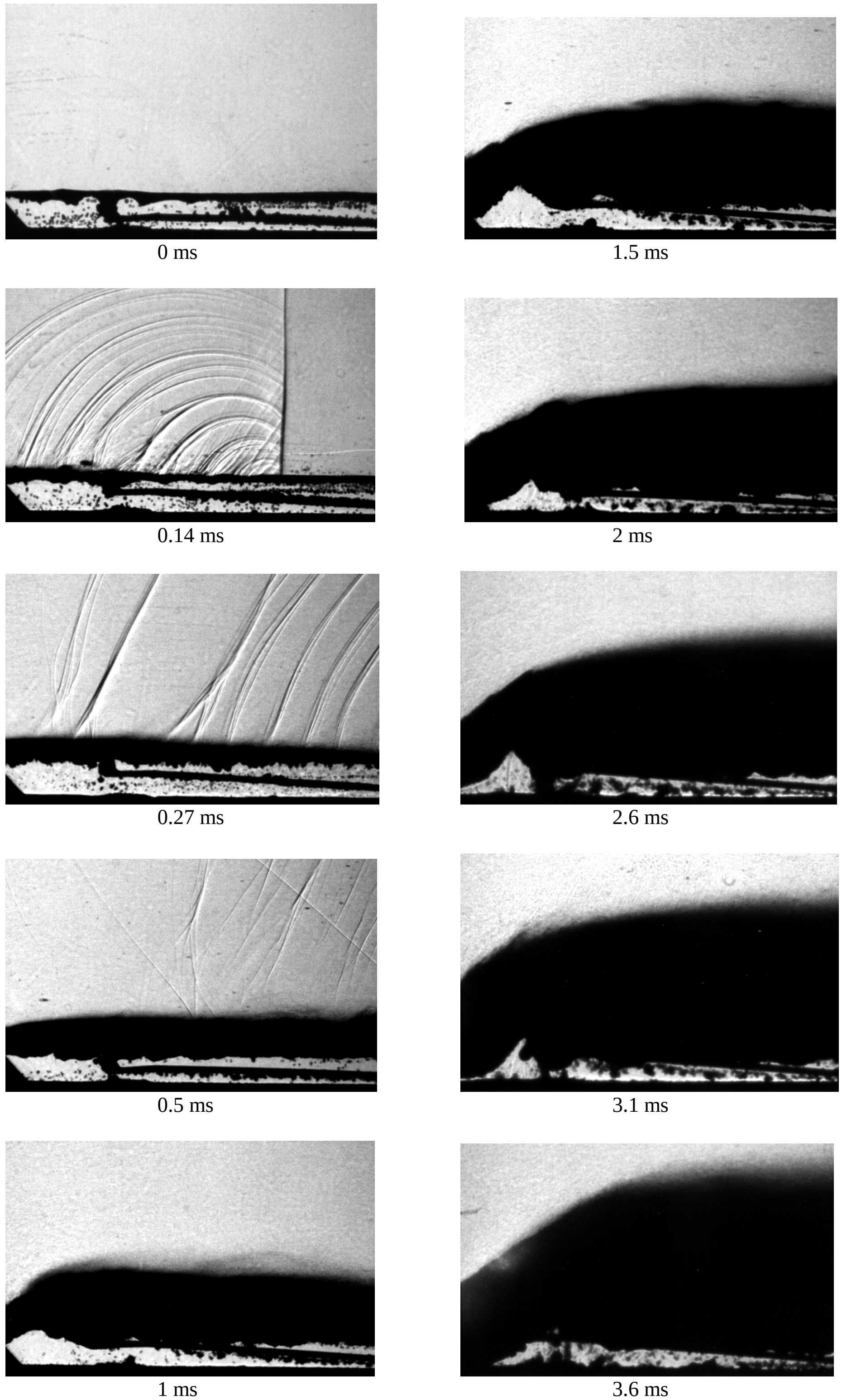

Figure 35: Shadowgraphs showing shock wave propagation, mist and wave development on water surface, $M_s = 2.3$, initial pressure 0.25 atm, initially rippled water surface. Air flow is from left to right in these images.

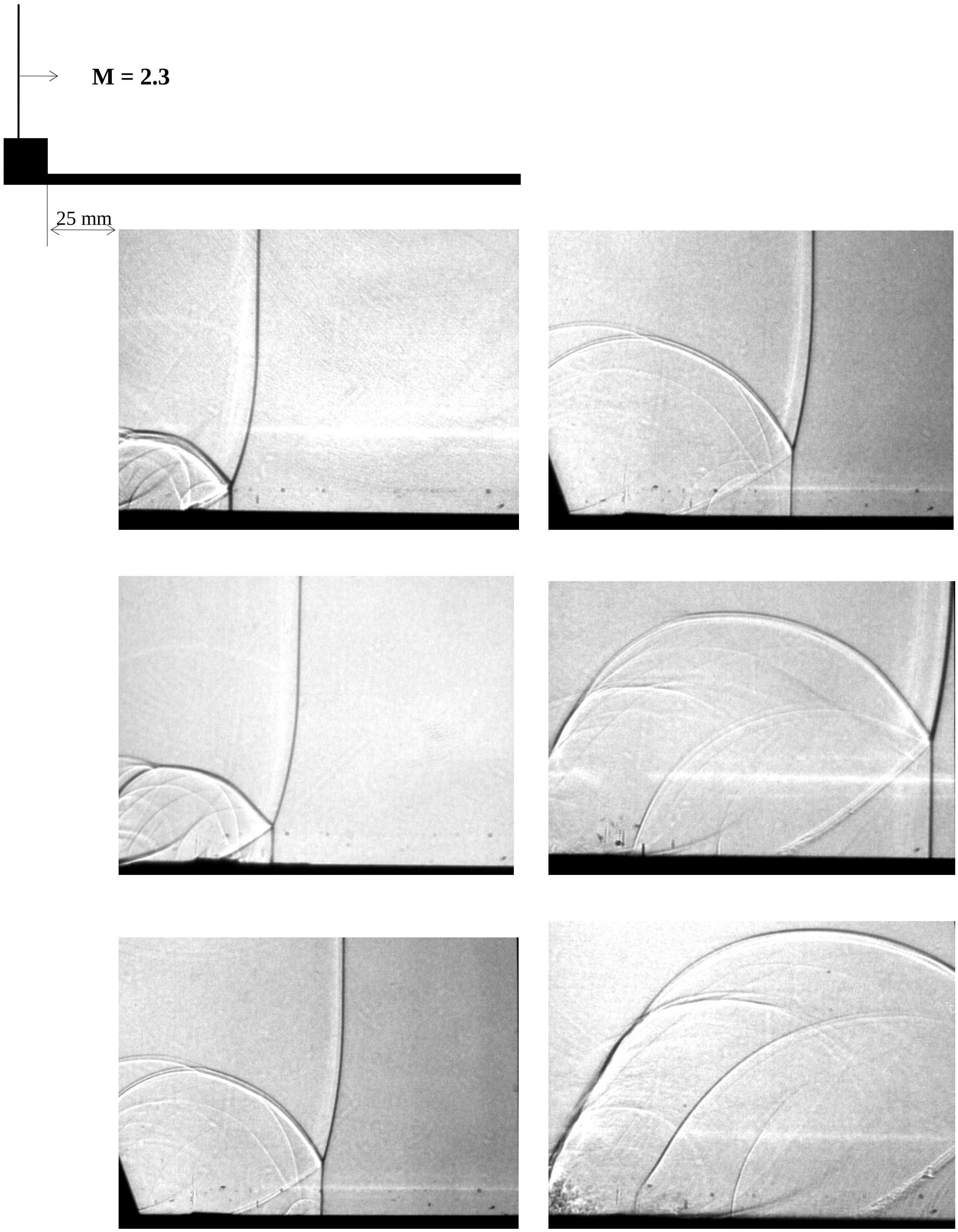

Figure 36: Shadowgraphs showing shock wave propagation over cavity with diffraction over backward facing step, $M_s = 2.3$, initial pressure 0.25 atm, no water.